Finite element discretization of two immiscible fluids with surface tension

Christine Bernardi, Sarra Maarouf, Driss Yakoubi

Finite element discretization of two immiscible fluids with surface tension

by Christine Bernardi[†] , Sarra Maarouf[†] and Driss Yakoubi[†]

Abstract. We consider a model for the flow of two immiscible fluids where the surface tension between both of them is taken into account. We first write the variational formulation of the problem and investigate its well-posedness. Next, we consider a finite element discretization of it and prove optimal a priori error estimates. Numerical experiments confirm its good properties.

Résumé. Nous considérons un modèle pour l'écoulement de deux fluides immiscibles où la tension de surface entre les deux fluides est prise en compte. Nous écrivons tout d'abord la formulation variationnelle de ce problème et vérifions qu'il est bien posé. Puis nous en proposons une discrétisation par éléments finis et prouvons des estimations d'erreur a priori qui s'avèrent optimales. Quelques expériences numériques confirment ses bonnes propriétés.

[†] CNRS, UMR 7598, Laboratoire Jacques-Louis Lions, F-75005, Paris, France.
Sorbonne Universités, UPMC Univ Paris 06, UMR 7598, LJLL, F-75005, Paris, France.
e-mail addresses: bernardi@ann.jussieu.fr, maarouf@ljll.math.upmc.fr, yakoubi@giref.ulaval.ca

1. Introduction.

Numerical methods for solving free surface problems are of great importance in many engineering applications and still a challenging field. Problems with free surfaces appear in immiscible multi-fluids problems, motion of glaciers, fluid structure interactions, blood in moving arteries and many other domains.

For two immiscible Newtonian fluids, the time-dependent Navier-Stokes equations govern the fluid motion in both fluids. Each fluid has a constant density and viscosity. As we are dealing with flow with more than one fluid, the surface tension at the fluid interface has to be accounted for. The surface tension is modeled as a body force concentrated at the interface by employing the Continuum Surface Force (CSF) model of Brackbill et al. [7]. The CSF model allows us to treat the dynamic boundary condition at the interface implicitly. So, the main difficulty in this problem is that, of course, each fluid flows through a time-dependent domain and that the interface is involved in the Navier-Stokes equations via the surface tension of the fluids. Moving interfaces can be handled with the Level Set method introduced S. Osher and al. [23], [30], see also [22] for a more general review of all these results.

It should be noted that the level set method is one of several interface-tracking techniques used routinely for two immiscible incompressible flow simulations. Others are the front-tracking method, see for instance [26], [33], the boundary integral method [17], and the volume-of-fluid (VOF) method [7], [19], [20]. Unfortunately, the main advantages of the level set method compared with other techniques are

- the attractive simplicity of its mathematical formulation and computing, and
- the ability of the method to simulate complex interfacial flows with strong surface tension effects.

In the level set method, the surface tension force, which is essentially a surface force, is traditionally modeled as a distributed body force, though concentrated in a band around the interface and arranged in such a way that the force has a maximum on the interface and decays rapidly with distance from it, see [30], [29].

Furthermore, in [11], the size of this band ε can be taken proportional to the mesh size h as $\varepsilon \approx 1.5\,h$. Thus, the variation of the surface tension across the interface may be described in terms of a regularized (smoothed) delta function with compact support. This approach removes the interface singularity from the standard continuum fluid flow equations, and ultimately allows the surface tension to be modeled using standard numerical techniques on Eulerian grids. The jump in phase properties across the interface, such as density and viscosity, is correspondingly modeled using a regularized Heaviside function.

So the full model consists in the time-dependent Navier–Stokes equations and a transport equation for the interface. A detailed description of a similar model can be found in [12], see also the references therein.

To our knowledge, the literature that studied the subject has been focussed on numerical validation and computational topics, while numerical analysis, for instance using fnite element method does not appear,

In this work, we investigate the main properties of the model and in particular the existence of a solution in the non-realistic case where the velocity satisfies homogeneous boundary conditions. Next, we propose a discretization of it by the characteristics method in time (indeed each equation contains a convection term) and standard conforming finite elements in space. We perform the a priori analysis of the discrete problem and prove nearly optimal estimates of the error. We finally present some numerical experiments that confirm the interest of both the model and its discretization.

The outline of the paper is as follows:
• In Section 2, we explain and write the model.
• In Section 3, we write its variational formulation and investigate its well-posedness.
• Section 4 is devoted to the description of the discretization and the well-posedness of the discrete problem.
• Its a priori analysis is performed in Section 5.
• In Section 6, we present some numerical experiments.

2. Mathematical description.

Let Ω be a bounded connected open set in $\mathbb{R}^d$, $d = 2$ or 3, with a Lipschitz-continuous boundary $\partial\Omega$. Let also T_f be a positive real number. If we assume a domain Ω with two immiscible fluids F_i, $i = 1, 2$, then the time dependent subdomains $\Omega_i(t)$, $t \in (0, T_f)$ are bounded by an external boundary $\partial\Omega$ and by a dynamic interface $\Gamma(t)$, see Figure 1. We assume that both fluids are homogeneous and therefore the physical properties are constant in each Ω_i which are a bounded connected domain with a Lipschitz–continuous and connected boundary $\partial\Omega_i(t)$:

$$\overline{\Omega} = \overline{\Omega}_1(t) \cup \overline{\Omega}_2(t), \qquad \Omega_1(t) \cap \Omega_2(t) = \emptyset. \tag{2.1}$$

We also define the interface between the two fluids

$$\Gamma(t) = \partial\Omega_1(t) \cap \partial\Omega_2(t). \tag{2.2}$$

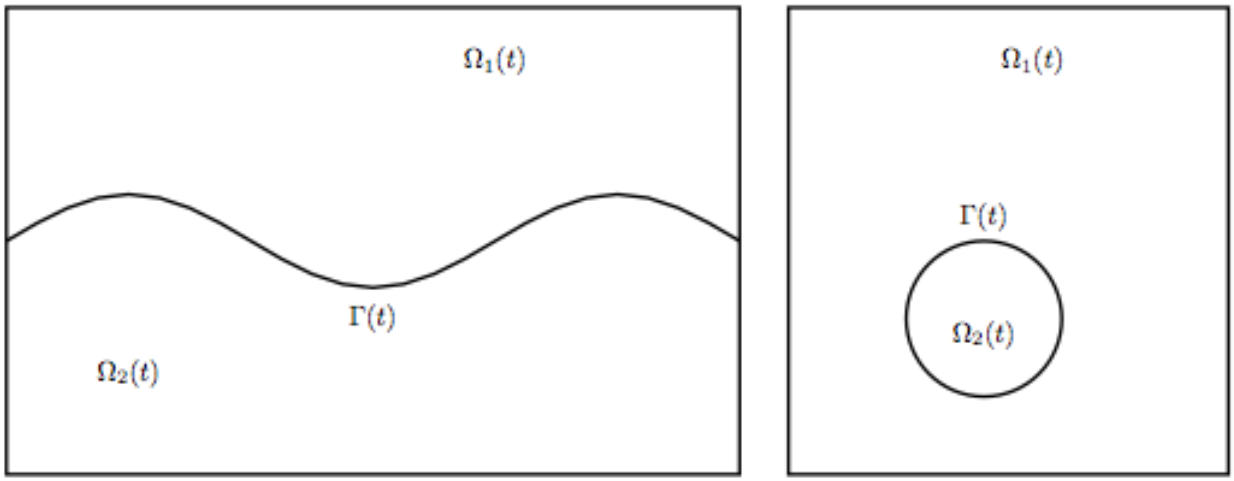

Figure 1. Two examples of domain Ω.

Then, the standard model for isothermal two immiscible flows can be described by the incompressible Navier-Stokes system

$$\begin{cases} \rho\left(\frac{\partial \boldsymbol{u}}{\partial t} + \boldsymbol{u} \cdot \nabla \boldsymbol{u}\right) + \nabla p - \nabla \cdot (\nu \nabla \boldsymbol{u}) = \boldsymbol{f} + \boldsymbol{f}_\sigma & \text{in } \Omega \times (0, T_f), \\ \nabla \cdot (\rho \boldsymbol{u}) = 0 & \text{in } \Omega \times (0, T_f), \end{cases} \tag{2.3}$$

which contain an additional force term $\boldsymbol{f}_\sigma$ due to the surface tension σ at the free interface $\Gamma(t)$. The unknowns are the velocity $\boldsymbol{u}$ (more precisely, each $\boldsymbol{u}_i = \boldsymbol{u}|_{\Omega_i}$ is the velocity of the fluid F_i, $i = 1, 2$) and the pressure p, $\boldsymbol{f}$ denotes any body force such as gravitational acceleration. Note that the density ρ as well as the viscosity ν are variable and discontinuous, that is

$$\rho = \begin{cases} \rho_1 & \text{in } \Omega_1 \times (0, T_f), \\ \rho_2 & \text{in } \Omega_2 \times (0, T_f), \end{cases} \quad \text{and} \quad \nu = \begin{cases} \nu_1 & \text{in } \Omega_1 \times (0, T_f), \\ \nu_2 & \text{in } \Omega_2 \times (0, T_f), \end{cases}$$

where each ρ_i and ν_i are nonnegative constants. Thus, the second equation in (2.3) can equivalently be written

$$\nabla \cdot \boldsymbol{u} = 0 \qquad \text{in } \Omega \times (0, T_f). \tag{2.4}$$

Surface tension effects are taken into account through the following force balance at the interface $\Gamma(t)$

$$\boldsymbol{u}_1 = \boldsymbol{u}_2 \qquad \text{on } \Gamma(t).$$

and

$$(\nu_1 \nabla \boldsymbol{u}_1 - p_1 I) \cdot \boldsymbol{n} + (\nu_2 \nabla \boldsymbol{u}_2 - p_2 I) \cdot \boldsymbol{n} = \sigma \kappa \boldsymbol{n} \qquad \text{on } \Gamma(t).$$

Here $\boldsymbol{n}$ is the unit normal at the interface pointing for instance into Ω_2, $\sigma \geq 0$ is the surface tension coefficient and $\kappa = \nabla \cdot \boldsymbol{n}$ is the curvature of the interface $\Gamma(t)$. The first condition implies continuity of the velocity across the interface, whereas the second describes the force balance on $\Gamma(t)$. To handle the curvature term, it is often to rewrite it as a volume force, that means

$$\boldsymbol{f}_\sigma = \sigma \kappa \boldsymbol{n} \delta_\sigma$$

where δ_σ is the Dirac delta function localizing the surface tension forces to the interface $\Gamma(t)$. In Lafaurie et al. [19], the authors propose an other shape but still equivalent to this force by introducing the projection operator in the tangent plan: $I - \boldsymbol{n} \otimes \boldsymbol{n}$ and then writing

$$\boldsymbol{f}_\sigma = -\nabla \cdot T, \qquad \text{such that} \qquad T = \sigma (I - \boldsymbol{n} \otimes \boldsymbol{n}) \delta_\sigma.$$

According to the applied Continuous Surface Force (CSF) approach, see [7], we introduce the following smooth regularization of the Heaviside function for a small $\varepsilon > 0$,

$$H_\varepsilon(\psi) = \begin{cases} 0 & \text{if } \psi < -\varepsilon, \\ \frac{1}{2}\big(1 + \frac{\psi}{\varepsilon} + \frac{1}{\pi} \sin(\frac{\pi \psi}{\varepsilon})\big) & \text{if } -\varepsilon \leq \psi \leq \varepsilon, \\ 1 & \text{if } \psi > \varepsilon. \end{cases} \tag{2.5}$$

On the other hand, following [30], a level set approach is employed to capture the interface $\Gamma(t)$. So, we consider the oriented distance function φ to $\Gamma(t)$ (also called level set function). The interface between the two fluids is then identified as the zero level of φ, more precisely

$$\Gamma(t) = \big\{ \boldsymbol{x} \in \overline{\Omega};\ \varphi(\boldsymbol{x}, t) = 0 \big\}.$$

Then, the smoothed density ρ and the viscosity ν are now given by

$$\rho(\varphi) = \rho_1 + (\rho_2 - \rho_1) H_\varepsilon(\varphi), \tag{2.6}$$

$$\nu(\varphi) = \nu_1 + (\nu_2 - \nu_1) H_\varepsilon(\varphi). \tag{2.7}$$

Since φ is a distance function (so that $\nabla \varphi$ is a normal vector to the interface $\Gamma(t)$) and using the well-known expressions, this tensor T can also be written as a function of φ, as follows:

$$T(\varphi) = \sigma \frac{dH_\varepsilon(\varphi)}{d\varphi} (I - \nabla \varphi \otimes \nabla \varphi), \tag{2.8}$$

where $\nabla\varphi \otimes \nabla\varphi$ stands for the tensor with coefficients $\partial_{x_i}\varphi\,\partial_{x_j}\varphi$, $1 \le i, j \le d$.

We recall that the unit normal $\boldsymbol{n}$ to the interface is classically obtained via φ : On the curve $\Gamma(t)$ with equation $\varphi = 0$,

$$\boldsymbol{n} = \frac{\nabla\varphi}{|\nabla\varphi|}.$$

Finally, the governing equations which describe two immiscible fluids with surface tension can be writing as a coupled time-dependent Navier–Stokes equations with transport equation:

$$\begin{cases} \rho(\varphi)\left(\frac{\partial \boldsymbol{u}}{\partial t} + \boldsymbol{u}\cdot\nabla\boldsymbol{u}\right) + \nabla p - \nabla\cdot(\nu(\varphi)\nabla\boldsymbol{u})) + \nabla\cdot T(\varphi) = \boldsymbol{f} & \text{in } \Omega\times(0,T_f), \\ \nabla\cdot\boldsymbol{u} = 0 & \text{in } \Omega\times(0,T_f), \\ \frac{\partial\varphi}{\partial t} + \boldsymbol{u}\cdot\nabla\varphi = 0 & \text{in } \Omega\times(0,T_f). \end{cases} \tag{2.9}$$

The last equation means that the interface $\Gamma(t)$ is convected by the fluid, see [12, eq. (7)]. A very similar model is considered in [9, eq. (2.9)], see also [21].

To make the problem complete, we enforce suitable boundary and initial conditions. The Dirichlet condition is imposed to the velocity and the level set function

$$\boldsymbol{u} = \boldsymbol{u}_D \quad \text{on } \partial\Omega \qquad \text{and} \qquad \varphi = \varphi_D \quad \text{on } \Gamma_{\boldsymbol{u}}, \tag{2.10}$$

where $\Gamma_{\boldsymbol{u}}$ denotes the part of boundary where the fluid goes in

$$\Gamma_{\boldsymbol{u}} = \{\boldsymbol{x}\in\partial\Omega;\, \boldsymbol{u}(\boldsymbol{x},t)\cdot\boldsymbol{n}(\boldsymbol{x}) < 0\},$$

and the initial conditions obviously read

$$\boldsymbol{u}(\boldsymbol{x},0) = \boldsymbol{u}_0(\boldsymbol{x}) \quad \text{and} \quad \varphi(\boldsymbol{x},0) = \varphi_0(\boldsymbol{x}) \qquad \text{for a.e. } \boldsymbol{x}\in\Omega. \tag{2.11}$$

The existence of $\Gamma_{\boldsymbol{u}}$ and the boundary condition on φ come from the nature of the third line of (2.9) which is a hyperbolic equation. However, in the case of homogeneous Dirichlet condition on $\partial\Omega$ for $\boldsymbol{u}$, no essential boundary conditions are needed on the level set function.

Certain compatibility conditions must be satisfied by the given data, mainly

$$\nabla\cdot\boldsymbol{u}_0 = 0 \quad \text{in } \Omega \qquad \text{and} \qquad \boldsymbol{u}_D(\cdot,0)\cdot\boldsymbol{n} = \boldsymbol{u}_0\cdot\boldsymbol{n} \quad \text{on } \partial\Omega, \tag{2.12}$$

in order to ensure the smoothness of the solution. From now on, we take φ negative on $\Omega_1(t)$ and positive on $\Omega_2(t)$, whence some compatibility conditions on φ_0 and φ_D.

3. Variational formulation and well-posedness.

Of course, our dream would be that problem (2.9) provided with the initial conditions (2.10) and the boundary conditions (2.11) is well-posed. However this seems impossible, for the two following reasons:
1) very few existence results are known for the transport equation (third line in (2.9)) when the velocity $\boldsymbol{u}$ does not vanish on the boundary and they require too much regularity of the domain;
2) the uniqueness of the solution of the time-dependent Navier-Stokes equation (first and second lines in (2.9)) is actually unknown in dimension $d = 3$.
So, we restrict ourselves to a simpler case.

In what follows, we use the whole scale of Sobolev spaces $W^{m,p}(\Omega)$, with $m \geq 0$ and $1 \leq p \leq +\infty$, equipped with the norm $\|\cdot\|_{W^{m,p}(\Omega)}$ and seminorm $|\cdot|_{W^{m,p}(\Omega)}$, with the usual notation $H^m(\Omega)$ when $p = 2$. We also need the space $H^1_0(\Omega)$ of functions in $H^1(\Omega)$ vanishing on $\partial\Omega$. For any separable Banach space E equipped with the norm $\|\cdot\|_E$, we denote by $\mathscr{C}^0(0,T;E)$ the space of continuous functions from $[0,T]$ with values in E. For each integer $m \geq 0$, we also introduce the space $H^m(0,T;E)$ as the space of measurable functions on $]0,T[$ with values in E such that the mappings: $v \mapsto \|\partial_t^\ell v\|_E$, $0 \leq \ell \leq m$, are square-integrable on $]0,T[$. We refer to [1] for the main properties of all these spaces.

Let us first consider the transport equation. In the case where $\boldsymbol{u}_D$ is not zero, the only existence result can be found in [6, Thm VI.1.6] but it requires too much regularity of the domain Ω and of the velocity $\boldsymbol{u}$. So, even if the case $\boldsymbol{u}_D \cdot \boldsymbol{n} = 0$ was treated in [10, Section IV.4], from now on we assume that

$$\boldsymbol{u}_D = \boldsymbol{0}. \tag{3.1}$$

With this condition, it is rather easy to prove the existence of a solution via the characteristics method, see [2, Thm II.7.6]. We are thus in a position to state the result concerning this equation.

Proposition 3.1. *Assume that the function $\boldsymbol{u}$ is divergence-free and satisfies*

$$\boldsymbol{u} \in \mathscr{C}^0(0,T_f;H^1_0(\Omega)^d) \cap \mathscr{C}^0(0,T_f;W^{1,\infty}(\Omega)^d). \tag{3.2}$$

Then, for any datum φ_0 in $L^2(\Omega)$, the problem

$$\begin{cases} \frac{\partial \varphi}{\partial t} + \boldsymbol{u} \cdot \nabla \varphi = 0 & \text{in } \Omega \times (0,T_f), \\ \\ \varphi(\cdot,0) = \varphi_0 & \text{in } \Omega, \end{cases} \tag{3.3}$$

admits a unique solution φ in $\mathscr{C}^0(0,T_f;L^2(\Omega))$. Moreover, this solution satisfies

$$\sup_{0 \leq t \leq T_f} \|\varphi(\cdot,t)\|_{L^2(\Omega)} \leq \|\varphi_0\|_{L^2(\Omega)}. \tag{3.4}$$

Proof. We establish successively the existence, the uniqueness and the stability property (3.4) of the solution.

1) Existence: Owing to the property (3.2) of $\boldsymbol{u}$, applying the Cauchy–Lipschitz theorem [28, Th. 21.1] yields that there exists for every pair $(\boldsymbol{x}, t)$ in $\Omega \times [0, T_f]$, a characteristic function $X = X(\boldsymbol{x}, t; \cdot)$ in $\mathscr{C}^0(0, T; \mathbb{R}^d)$ solution of the ordinary differential equation

$$\begin{cases} \frac{dX}{dt} = \boldsymbol{u} \circ X & \text{in } \Omega \times (0, T_f), \\ X(\boldsymbol{x}, t; t) = \boldsymbol{x} & \text{in } \Omega. \end{cases}$$

Thus, it is readily checked that the function φ defined by

$$\varphi(\boldsymbol{x}, t) = \varphi_0(X(\boldsymbol{x}, 0; t)), \tag{3.5}$$

is a solution of problem (3.3).
2) Uniqueness: Let φ_1 and φ_2 be two solutions of problem (3.3). Setting $\varphi = \varphi_1 - \varphi_2$ and multiplying the difference of the two equations by φ gives

$$\frac{1}{2}\frac{\partial \varphi^2}{\partial t} + \frac{1}{2}\boldsymbol{u} \cdot \nabla \varphi^2 = 0.$$

Since $\boldsymbol{u}$ is divergence-free and vanishes on the boundary, integrating on Ω yields

$$\frac{1}{2}\frac{d\|\varphi\|^2_{L^2(\Omega)}}{dt} = 0,$$

whence, since $\varphi(\cdot, 0)$ is zero, $\varphi(\cdot, t)$ is zero. Thus, φ_1 and φ_2 coincide.
3) Stability: Multiplying as previously problem (3.3) by φ and integrating on Ω leads to

$$\frac{d\|\varphi\|^2_{L^2(\Omega)}}{dt} = 0,$$

whence property (3.4).

It follows from formula (3.5) that the regularity of the solution φ only depends on that of $\boldsymbol{u}$ and φ_0. So we state the regularity properties that we need to study the full problem.

Corollary 3.2. *If the assumptions of Proposition* 3.1 *hold, for any real number* p, $1 \leq p < \infty$, *and any datum* φ_0 *in* $W^{1,p}(\Omega)$, *the solution* φ *of problem* (3.3) *belongs to* $\mathscr{C}^0(0, T_f; W^{1,p}(\Omega))$.

We now consider the Navier-Stokes equations. We first write their variational formulation:

Find $\boldsymbol{u}$ *in* $L^2(0, T; H^1_0(\Omega)^d) \cap \mathscr{C}^0(0, T; L^2(\Omega)^d)$ *and* p *in* $L^2(0, T; L^2(\Omega))$ *such that*

$$\boldsymbol{u}(\cdot, 0) = \boldsymbol{u}_0, \tag{3.6}$$

and, for a.e. t *in* $[0, T]$,

$$\begin{aligned} \forall \boldsymbol{v} \in H^1_0(\Omega)^d, \quad & \int_\Omega \rho(\varphi)(\boldsymbol{x}) \left(\frac{\partial \boldsymbol{u}}{\partial t} + \boldsymbol{u} \cdot \nabla \boldsymbol{u} \right)(\boldsymbol{x}) \boldsymbol{v}(\boldsymbol{x})\, d\boldsymbol{x} - \int_\Omega (\nabla \cdot \boldsymbol{v})(\boldsymbol{x}) p(\boldsymbol{x})\, d\boldsymbol{x} \\ & + \int_\Omega \nu(\varphi)(\boldsymbol{x}) \nabla \boldsymbol{u}(\boldsymbol{x}) : \nabla \boldsymbol{v}(\boldsymbol{x})\, d\boldsymbol{x} - \int_\Omega T(\varphi)(\boldsymbol{x}) : \nabla \boldsymbol{v}(\boldsymbol{x})\, d\boldsymbol{x} = \langle \boldsymbol{f}, \boldsymbol{v} \rangle, \end{aligned} \tag{3.7}$$

$$\forall q \in L^2(\Omega), \quad \int_\Omega (\nabla \cdot \boldsymbol{u})(\boldsymbol{x}) q(\boldsymbol{x})\, d\boldsymbol{x} = 0,$$

where $\langle \cdot, \cdot \rangle$ denotes the duality pairing between $H_0^1(\Omega)^d$ and its dual space $H^{-1}(\Omega)^d$. The arguments for proving its equivalence with the first two lines of (2.9) are fully standard, so we skip them.

First, we note from the definitions (2.6) and (2.7) that, for any φ,

$$\min\{\rho_1, \rho_2\} \le \rho(\varphi) \le \max\{\rho_1, \rho_2\}, \qquad \min\{\nu_1, \nu_2\} \le \nu(\varphi) \le \max\{\nu_1, \nu_2\}. \tag{3.8}$$

Next, since $\frac{dH_\varepsilon}{d\varphi}$ is bounded independently of φ, for any φ in $L^4(0, T_f; W^{1,4}(\Omega))$, the quantity $T(\varphi)$ belongs to $L^2(0, T_f; L^2(\Omega)^{d\times d})$. So all the terms in problem (3.7) are well-defined. Moreover, thanks to all these properties, the existence of a solution for problem (3.7) is derived by exactly the same arguments as for the standard Navier–Stokes equations. So we refer to [31, Chap. III, Thms 3.1 & 3.2] and [13, Chap. V, Thms 1.4 & 1.5] for the next result.

Proposition 3.3. *Assume that the function φ belongs to $L^4(0, T_f; W^{1,4}(\Omega))$. Then, for any datum $\boldsymbol{f}$ in $L^2(0, T_f; H^{-1}(\Omega)^d)$ and $\boldsymbol{u}_0$ in $L^2(\Omega)^d$ satisfying*

$$\nabla \cdot \boldsymbol{u}_0 = 0 \quad \text{in } \Omega \qquad \text{and} \qquad \boldsymbol{u}_0 \cdot \boldsymbol{n} = 0 \quad \text{on } \partial\Omega, \tag{3.9}$$

problem (3.6) − (3.7) has at least a solution $(\boldsymbol{u}, p)$. Moreover, in dimension $d = 2$, this solution is unique, up to an additive constant on the pressure.

Unfortunately, it seems difficult to prove, specially in dimension $d = 3$, that this solution satisfies the regularity properties required in Proposition 3.1 (even if they could be weakened). Up to our knowledge, the only existence result for the full problem (3.3) − (3.6) − (3.7) is due to Milcent [21, Chap. IV, Th. 1]; we only quote it and refer to [21, Chap. IV] and [9, Thm 2.2] for its proof (which relies on space and time regularization).

Proposition 3.4. *Let Ω be a bounded smooth domain in $\mathbb{R}^3$, and let p be a real number > 3. We consider data*
(i) φ_0 in $W^{2,p}(\Omega)$ such that $|\nabla\varphi_0|$ is larger than a positive constant in a neighbourhood of $\{\boldsymbol{x} \in \Omega;\ \varphi_0(\boldsymbol{x}) = 0\}$;
(ii) $\boldsymbol{f}$ equal to $\sigma d \frac{dH_\varepsilon(\varphi)}{d\varphi}$,
(iii) $\boldsymbol{u}_0$ in $W^{2,p}(\Omega)^d \cap W_0^{1,p}(\Omega)^d$ which is divergence-free in Ω.
Then, there exists a positive number T_* only depending on the initial data such that problem (3.3) − (3.6) − (3.7) has a solution in $\Omega \times [0, T_*]$. Moreover, this solution satisfies

$$\varphi \in L^\infty(0, T_*; W^{2,p}(\Omega)),$$
$$\boldsymbol{u} \in L^\infty(0, T_*; W_0^{1,p}(\Omega)^d) \cap L^p(0, T_*; W^{2,p}(\Omega)^d),$$
$$\nabla p \in L^p(0, T_*; L^p(\Omega)^d).$$

Even if neither the assumptions of this proposition nor the results are very realistic, it leaves the hope that the problem we work with is not fully incoherent.

4. The discrete problem and its well-posedness.

To describe the discrete problem, we first need some notation. Next, we write it and prove its well-posedness.

4.1. Some notation.

Since we intend to work with non-uniform time steps, we introduce a partition of the interval $[0, T_f]$ into subintervals $[t_{n-1}, t_n]$, $1 \leq n \leq N$, with $0 = t_0 < t_1 < \cdots < t_N = T_f$. We denote by τ_n the time step $t_n - t_{n-1}$, by τ the N-tuple $(\tau_1, \ldots, \tau_N)$ and by $|\tau|$ the maximum of the τ_n, $1 \leq n \leq N$.

We assume that Ω is a polygon ($d = 2$) or a polyhedron ($d = 3$). For $0 \leq n \leq N$, let $(\mathcal{T}_h^n)_h$ be a regular family of triangulations of Ω (by triangles or tetrahedra), in the sense that, for each h:
• $\overline{\Omega}$ is the union of all elements of $\mathcal{T}_h^n$;
• The intersection of two different elements of $\mathcal{T}_h^n$, if not empty, is a vertex or a whole edge or a whole face of both of them;
• The ratio of the diameter h_K of any element K of $\mathcal{T}_h^n$ to the diameter of its inscribed circle or sphere is smaller than a constant independent of h and n.
As usual, h_n stands for the maximum of the diameters h_K, $K \in \mathcal{T}_h^n$. We also denote by $\mathcal{V}_h^n$ the set of all vertices of elements of $\mathcal{T}_h^n$. In what follows, c, c', ... are generic constants which may vary from line to line but are always independent of the τ_n and h_n.

We have decided to work with the Taylor–Hood finite element introduced in [16]. So, denoting by $\mathcal{P}_k(K)$ the space of restrictions to K of polynomials with d variables and total degree $\leq k$, we consider the finite element spaces

$$\mathbb{Y}_h^n = \big\{ \boldsymbol{v}_h \in H^1(\Omega);\ \forall K \in \mathcal{T}_h^n,\ \boldsymbol{v}_h|_K \in \mathcal{P}_2(K) \big\}, \quad \mathbb{X}_h^n = (\mathbb{Y}_h^n)^d \cap H_0^1(\Omega)^d, \tag{4.1}$$

and

$$\mathbb{M}_h^n = \big\{ q_h \in H^1(\Omega);\ \forall K \in \mathcal{T}_h^n,\ q_h|_K \in \mathcal{P}_1(K) \big\}. \tag{4.2}$$

We denote by $\mathcal{I}_h^n$ the Lagrange interpolation operator at the nodes of $\mathcal{V}_h^n$ with values in $\mathbb{M}_h^n$.

4.2. Discretization of the transport equation.

For reasons which appear later on, we still work with homogeneous boundary condition on the velocity, i.e. we assume that (3.1) holds. We have decided to use the characteristics method to discretize the transport equation, as introduced and firstly analyzed in [24].

Assuming that the datum φ_0 is continuous on $\overline{\Omega}$, we simply define

$$\varphi_h^0 = \mathcal{I}_h^0 \varphi_0. \tag{4.3}$$

Next, at time t_n, assuming that $\boldsymbol{u}_h^{n-1}$ and φ_h^{n-1} are known, we define for all $\boldsymbol{x}$ in $\mathcal{V}_h^n$

$$\boldsymbol{x}_h^n = \boldsymbol{x} - \tau_n\, \boldsymbol{u}_h^{n-1}(\boldsymbol{x}), \tag{4.4}$$

thus, we define $\tilde{\varphi}_h^n$ by

$$\tilde{\varphi}_h^n(\boldsymbol{x}) = \varphi_h^{n-1}(\boldsymbol{x}_h^n), \tag{4.5}$$

and finally

$$\varphi_h^n = \mathcal{I}_h^n \tilde{\varphi}_h^n. \tag{4.6}$$

The simplicity of this algorithm is obvious. Note simply that:
(i) If $\boldsymbol{x}$ belongs to $\partial\Omega$, the fact that $\boldsymbol{u}_h^{n-1}$ belongs to $H_0^1(\Omega)^d$ implies that $\boldsymbol{x}_h^n$ is equal to $\boldsymbol{x}$, hence belongs to $\overline{\Omega}$;
(ii) otherwise, τ_n must be chosen small enough for $\boldsymbol{x}_h^n$ to be in $\overline{\Omega}$.
This condition is made precise later on.

Remark 4.1. Since the function φ_h^n is continuous on $\overline{\Omega}$, we can define the curve

$$\Gamma_h^n = \big\{\boldsymbol{x} \in \overline{\Omega};\ \varphi_h^n(\boldsymbol{x}) = 0\big\}. \tag{4.7}$$

We hope that this curve is a good approximation of the interface $\Gamma(t)$ at time $t = t_n$. This will be investigated later on.

4.3. Discretization of the Navier–Stokes equations.

This discretization relies on two arguments: using the characteristics method for handling the convection term and a Galerkin method for the rest of the equation. As previously, assuming that the datum $\boldsymbol{u}_0$ is continuous on $\overline{\Omega}$, we simply define

$$\boldsymbol{u}_h^0 = \mathcal{I}_h^0 \boldsymbol{u}_0. \tag{4.8}$$

Next, at time t_n, $1 \le n \le N$, assuming that $\boldsymbol{u}_h^{n-1}$ and φ_h^n are known, still relying on equation (4.4), we define $\tilde{\boldsymbol{u}}_h^{n-1}$ as the interpolate in $(\mathbb{M}_h^n)^d$ of the values $\boldsymbol{u}_h^{n-1}(\boldsymbol{x}_h^n)$ at all nodes of $\mathcal{V}_h^n$ which belong to Ω. Then, the discrete problem reads:

Find $\boldsymbol{u}_h^n$ in $\mathbb{X}_h^n$ and p_h^n in $\mathbb{M}_h^n$ such that

$$\begin{aligned}
\forall \boldsymbol{v} \in \mathbb{X}_h^n, \quad & \int_\Omega \rho(\varphi_h^n)(\boldsymbol{x}) \left(\frac{\boldsymbol{u}_h^n - \tilde{\boldsymbol{u}}_h^{n-1}}{\tau_n} \right)(\boldsymbol{x}) \boldsymbol{v}(\boldsymbol{x})\, d\boldsymbol{x} - \int_\Omega (\nabla \cdot \boldsymbol{v})(\boldsymbol{x}) p_h^n(\boldsymbol{x})\, d\boldsymbol{x} \\
& + \int_\Omega \nu(\varphi_h^n)(\boldsymbol{x}) \nabla \boldsymbol{u}_h^n(\boldsymbol{x}) : \nabla \boldsymbol{v}(\boldsymbol{x})\, d\boldsymbol{x} - \int_\Omega T(\varphi_h^n)(\boldsymbol{x}) : \nabla \boldsymbol{v}(\boldsymbol{x})\, d\boldsymbol{x} = \langle \boldsymbol{f}(t_n), \boldsymbol{v} \rangle, \\
\forall q \in \mathbb{M}_h^n, \quad & \int_\Omega (\nabla \cdot \boldsymbol{u}_h^n)(\boldsymbol{x}) q(\boldsymbol{x})\, d\boldsymbol{x} = 0.
\end{aligned} \tag{4.9}$$

4.4. Well-posedness of the discrete problem.

To prove the well-posedness of problem (4.4) – (4.5) – (4.6), we must check that the $\boldsymbol{x}_h^n$ defined in (4.4) belongs to $\overline{\Omega}$. This is proved in [27, Prop. 1], see also [25, Rem. 3], when the following condition holds

$$\tau_n < \frac{1}{\|\boldsymbol{u}_h^{n-1}\|_{W^{1,\infty}(\Omega)^d}}. \tag{4.10}$$

However, we have no a priori control on the quantity $\|\boldsymbol{u}_h^{n-1}\|_{W^{1,\infty}(\Omega)^d}$. So we prefer to use the following modified algorithm:
1) if the quantity defined in (4.4) belongs to $\overline{\Omega}$, take $\boldsymbol{x}_h^n$ equal to it;
2) otherwise, take $\boldsymbol{x}_h^n$ equal to

$$\boldsymbol{x}_h^n = \boldsymbol{x} - t\,\boldsymbol{u}_h^{n-1}(\boldsymbol{x}), \tag{4.11}$$

for the smallest t in $[0, \tau_n]$ such that $\boldsymbol{x} - t\,\boldsymbol{u}_h^{n-1}(\boldsymbol{x})$ belongs to $\partial\Omega$.
Note that the modification introduced above is only used for a small number of nodes $\boldsymbol{x}$ which are very near to $\partial\Omega$. We are thus in a position to state the next proposition.

Proposition 4.2. *For any datum φ_0 continuous on Ω, problem* (4.4)(*or* (4.11)) – (4.5) – (4.6) *has a unique solution φ_h^n in $\mathbb{M}_h^n$.*

The well-posedness of problem (4.9) relies on standard arguments: Defining $\boldsymbol{x}_h^n$ by (4.4) or (4.11) as previously, we know $\tilde{\boldsymbol{u}}_h^{n-1}$. We also observe that the quantity $T(\varphi_h^n)$ belongs to $L^2(\Omega)^{d\times d}$. So the following result is readily checked.

Proposition 4.3. *For any datum $\boldsymbol{u}_0$ continuous on $\overline{\Omega}$, problem* (4.9) *has a unique solution $(\boldsymbol{u}_h^n, p_h^n)$ in $\mathbb{X}_h^n \times \mathbb{M}_h^n$, up to an additive constant on the pressure p_h^n.*

Proof. When φ_h^n (and $T(\varphi_h^n)$), $\tilde{\boldsymbol{u}}_h^{n-1}$ and $\boldsymbol{f}$ are known, this problem results in a square linear system. So it suffices to prove that the only solution of the problem

$$\begin{aligned}
&\forall \boldsymbol{v} \in \mathbb{X}_h^n, \quad \int_\Omega \rho(\varphi_h^n)(\boldsymbol{x}) \frac{\boldsymbol{u}_h^n(\boldsymbol{x})}{\tau_n} \boldsymbol{v}(\boldsymbol{x})\, d\boldsymbol{x} - \int_\Omega (\nabla\cdot\boldsymbol{v})(\boldsymbol{x}) p_h^n(\boldsymbol{x})\, d\boldsymbol{x} \\
&\qquad\qquad + \int_\Omega \nu(\varphi_h^n)(\boldsymbol{x}) \nabla\boldsymbol{u}_h^n(\boldsymbol{x}) : \nabla\boldsymbol{v}(\boldsymbol{x})\, d\boldsymbol{x} = 0, \\
&\forall q \in \mathbb{M}_h^n, \quad \int_\Omega (\nabla\cdot\boldsymbol{u}_h^n)(\boldsymbol{x}) q(\boldsymbol{x})\, d\boldsymbol{x} = 0,
\end{aligned}$$

is zero, up to an additive constant on the pressure p_h^n. By taking $\boldsymbol{v}$ equal to $\boldsymbol{u}_h^n$, combining the two previous equations and using (3.8), we easily derive that $\boldsymbol{u}_h^n$ is zero. Thus, the fact that p_h^n is a constant follows from the inf-sup condition, see for instance [14, Chap. II, Thm 4.2],

$$\forall q \in \mathbb{M}_h^n, \int_\Omega q(\boldsymbol{x})\, d\boldsymbol{x} = 0, \qquad \sup_{\boldsymbol{v}\in\mathbb{X}_h^n} \frac{\int_\Omega (\nabla\cdot\boldsymbol{v})(\boldsymbol{x}) q(\boldsymbol{x})\, d\boldsymbol{x}}{\|\boldsymbol{v}\|_{H^1(\Omega)^d}} \geq \beta\, \|q\|_{L^2(\Omega)}, \tag{4.12}$$

where the constant β is positive.

Remark 4.4. The main advantage of the discretization that we propose is that it uncouples the computation of the φ_h^n and of the $\boldsymbol{u}_h^n$. However, this can lead to a lack of convergence for too large time steps or in the case of time oscillations of the solution. To remedy this, we can use an iterative algorithm as follows: at each time t_n,
1) define $\varphi_h^{n,0}$ as equal to φ_h^{n-1} and $\boldsymbol{u}_h^{n,0}$ as equal to $\boldsymbol{u}_h^{n-1}$;
2) setting

$$\boldsymbol{x}_h^{n,k} = \boldsymbol{x} - \tau_n\, \boldsymbol{u}_h^{n,k-1}(\boldsymbol{x}),$$

(or the modified version (4.11)), we define $\varphi_h^{n,k}$ as the interpolate in $\mathbb{M}_h^n$ of the values $\varphi^{n,k-1}(\boldsymbol{x}_h^{n,k})$ at all nodes of $\mathcal{V}_h^n$ and similarly $\tilde{\boldsymbol{u}}_h^{n,k-1}$ as the interpolate in $\mathbb{M}_h^n$ of the values $\boldsymbol{u}^{n,k-1}(\boldsymbol{x}_h^{n,k})$ at all nodes of $\mathcal{V}_h^n$ which belong to Ω, next we solve

Find $\boldsymbol{u}_h^{n,k}$ *in* $\mathbb{X}_h^n$ *and* $p_h^{n,k}$ *in* $\mathbb{M}_h^n$ *such that*

$$\forall \boldsymbol{v} \in \mathbb{X}_h^n; \quad \int_\Omega \rho(\varphi_h^{n,k})(\boldsymbol{x}) \left(\frac{\boldsymbol{u}_h^{n,k} - \tilde{\boldsymbol{u}}_h^{n,k-1}}{\tau_n} \right)(\boldsymbol{x}) \boldsymbol{v}(\boldsymbol{x})\, d\boldsymbol{x} - \lambda_k \int_\Omega (\nabla \cdot \boldsymbol{v})(\boldsymbol{x}) p_h^{n,k}(\boldsymbol{x})\, d\boldsymbol{x}$$

$$+ \lambda_k \int_\Omega \nu(\varphi_h^{n,k})(\boldsymbol{x}) \nabla \boldsymbol{u}_h^{n,k}(\boldsymbol{x}) : \nabla \boldsymbol{v}(\boldsymbol{x})\, d\boldsymbol{x} - \lambda_k \int_\Omega T(\varphi_h^{n,k})(\boldsymbol{x}) : \nabla \boldsymbol{v}(\boldsymbol{x})\, d\boldsymbol{x} = \lambda_k \langle \boldsymbol{f}(t_n), \boldsymbol{v} \rangle,$$

$$\forall q \in \mathbb{M}_h^n, \quad \int_\Omega (\nabla \cdot \boldsymbol{u}_h^{n,k})(\boldsymbol{x}) q(\boldsymbol{x})\, d\boldsymbol{x} = 0.$$

The λ_k are positive parameters, chosen in order to ensure the consistency of the algorithm.
3) For a fixed integer K, we set: $\varphi^n = \varphi^{n,K}$ and $\boldsymbol{u}^n = \boldsymbol{u}^{n,K}$, and go back to step 1.
Of course, the parameter K must be chosen small enough, namely equal to 2 or 3, in order that the cost of this algorithm remains reasonable. Its analysis is nearly the same as for the previous problem (4.4) – (4.5) – (4.6) – (4.9), so that we skip it.

5. A priori error analysis.

In this section, we still work with $\boldsymbol{u}_D = \mathbf{0}$ and we admit that, for all $\boldsymbol{x}$ in $\mathcal{V}_h^n$, the $\boldsymbol{x}_h^n$ defined in (4.4) belong to $\overline{\Omega}$ (indeed, it is not so difficult in practice to satisfy condition (4.10): when $\|\boldsymbol{u}_h^{n-1}\|_{W^{1,\infty}(\Omega)^d}$ is larger, it is possible to work with a smaller τ_n in order to enforce this condition).

We first state a stability property for the discrete transport equation.

Lemma 5.1. *For any datum φ_0 continuous on $\overline{\Omega}$, the next property holds for $1 \leq n \leq N$*

$$\|\varphi_h^n\|_{L^\infty(\Omega)} \leq \|\varphi_0\|_{L^\infty(\Omega)}. \tag{5.1}$$

Proof. Since each φ_h^n belongs to $\mathbb{M}_h^n$, hence is piecewise affine, we have

$$\|\varphi_h^n\|_{L^\infty(\Omega)} = \max_{\boldsymbol{x}\in\mathcal{V}_h^n} |\varphi_h^n(\boldsymbol{x})|. \tag{5.2}$$

Thus it follows from (4.5) and (4.6) that

$$\|\varphi_h^n\|_{L^\infty(\Omega)} \leq \|\varphi_h^{n-1}\|_{L^\infty(\Omega)}.$$

By noting that

$$\|\mathcal{I}_h^0\varphi_0\|_{L^\infty(\Omega)} \leq \|\varphi_0\|_{L^\infty(\Omega)},$$

the desired result is derived by induction on n.

The error estimate is a little more tricky, even in the L^∞- norm. We refer to [25, Prop. 1] for a similar result in a different case.

Proposition 5.2. *Assume that the solution φ of problem* (3.3) *satisfies*

$$\varphi \in \mathscr{C}^0(0,T_f;W^{2,\infty}(\Omega)) \cap W^{1,\infty}(0,T_f;L^\infty(\Omega)). \tag{5.3}$$

Then the following estimate holds for $1 \leq n \leq N$

$$\|\varphi(\cdot,t_n) - \varphi_h^n\|_{L^\infty(\Omega)} \leq C\left(h_n^2 + \tau_n(1+\|\boldsymbol{u}_h^{n-1}\|_{L^\infty(\Omega)^d})\right) + \|\varphi(\cdot,t_{n-1}) - \varphi_h^{n-1}\|_{L^\infty(\Omega)}, \tag{5.4}$$

where the constant C only depends on the regularity of φ.

Proof. We start with the triangle inequality

$$\|\varphi(\cdot,t_n) - \varphi_h^n\|_{L^\infty(\Omega)} \leq \|\varphi(\cdot,t_n) - \mathcal{I}_h^n\varphi(\cdot,t_n)\|_{L^\infty(\Omega)} + \|\mathcal{I}_h^n\varphi(\cdot,t_n) - \varphi_h^n\|_{L^\infty(\Omega)}.$$

Bounding the first term in the right-hand side relies on standard results [4, Chap. IX, Lemme 1.1]. To bound the second one, we use (5.2) and for each $\boldsymbol{x}$ in $\mathcal{V}_h^n$, we compute

$$\begin{aligned}\mathcal{I}_h^n\varphi(\boldsymbol{x},t_n) - \varphi_h^n(\boldsymbol{x}) &= \varphi(\boldsymbol{x},t_n) - \varphi_h^{n-1}(\boldsymbol{x}_h^n)\\ &= \varphi(\boldsymbol{x},t_n) - \varphi(\boldsymbol{x}_h^n,t_{n-1}) + \varphi(\boldsymbol{x}_h^n,t_{n-1}) - \varphi_h^{n-1}(\boldsymbol{x}_h^n).\end{aligned}$$

From the definition of $\boldsymbol{x}_h^n$ and the Lipschitz continuity of φ, we derive

$$|\mathcal{I}_h^n\varphi(\boldsymbol{x},t_n)-\varphi_h^n(\boldsymbol{x})|\le c\tau_n(1+\|\boldsymbol{u}_h^{n-1}\|_{L^\infty(\Omega)^d})+\|\varphi(\cdot,t_{n-1})-\varphi_h^{n-1}\|_{L^\infty(\Omega)}$$

where c stands for the Lipschitz constant of φ on $\Omega\times]0,T_f[$. Combining all this gives the desired estimate.

In view of the quantity $T(\varphi)$, we also need an estimate for $\|\varphi(\cdot,t_n)-\varphi_h^n\|_{W^{1,4}(\Omega)}$.

Proposition 5.3. *Assume that, for a real number $p\ge 1$, the solution φ of problem* (3.3) *satisfies*

$$\varphi\in\mathscr{C}^0(0,T_f;W^{2,p}(\Omega)). \tag{5.5}$$

Then the following estimate holds for $1\le n\le N$

$$\begin{aligned}\|\varphi(\cdot,t_n)-\varphi_h^n\|_{W^{1,p}(\Omega)}\le C\,h_n+Ch_{n,\min}^{-1}\tau_n(1+\|\boldsymbol{u}_h^{n-1}\|_{L^\infty(\Omega)^d})\\ +ch_{n,\min}^{-1}\|\varphi(\cdot,t_{n-1})-\varphi_h^{n-1}\|_{L^\infty(\Omega)},\end{aligned} \tag{5.6}$$

where $h_{n,\min}$ stands for the minimum of the diameters h_K, $K\in\mathcal{T}_h^n$.

Proof. We start once more from the triangle inequality

$$\|\varphi(\cdot,t_n)-\varphi_h^n\|_{W^{1,p}(\Omega)}\le\|\varphi(\cdot,t_n)-\mathcal{I}_h^n\varphi(\cdot,t_n)\|_{W^{1,p}(\Omega)}+\|\mathcal{I}_h^n\varphi(\cdot,t_n)-\varphi_h^n\|_{W^{1,p}(\Omega)}.$$

and use [4, Chap. IX, Lemme 1.2] to evaluate the first term. On the other hand, denoting by $\psi_{\boldsymbol{x}}$ the Lagrange function associated with each node in $\mathcal{V}_h^n$, switching to the reference element to evaluate the norm of this function in $W^{1,p}(\Omega)$ and using the fact, due the regularity of the family of triangulations, the support of each $\psi_{\boldsymbol{x}}$ only intersects the support of a finite number of other ones, we derive

$$\|\mathcal{I}_h^n\varphi(\cdot,t_n)-\varphi_h^n\|_{W^{1,p}(\Omega)}^p\le c\sum_{\boldsymbol{x}\in\mathcal{V}_h^n}|\mathcal{I}_h^n\varphi(\boldsymbol{x},t_n)-\varphi_h^n(\boldsymbol{x})|^p\,h_{K_x}^{d-p}.$$

where $K_{\boldsymbol{x}}$ is any element of $\mathcal{T}_h^n$ containing $\boldsymbol{x}$. The maximmum of the $|\mathcal{I}_h^n\varphi(\boldsymbol{x},t_n)-\varphi_h^n(\boldsymbol{x})|$ has been evaluated in the previous proof. We derive from the regularity of the family of triangulations that

$$\sum_{\boldsymbol{x}\in\mathcal{V}_h^n}h_{K_x}^d\le c\,\mathrm{meas}(\Omega),$$

which leads to the desired result.

We are now interested in the evaluation of the error issued from the discrete Navier–Stokes equations. We refer to [5, Section 4.3] for this evaluation in a simpler case. We begin with the terms involving φ_h^n and, for simplicity, we denote by ε_1^n and ε_2^n the right-hand sides of estimates (5.4) and (5.6), respectively.

Lemma 5.4. *If the assumptions of Propositions* 5.2 *and* 5.3 *are satisfied, the following estimates hold for $1\le n\le N$*

$$\|\rho(\varphi(.,t_n))-\rho(\varphi_h^n)\|_{L^\infty(\Omega)}+\|\nu(\varphi(.,t_n))-\nu(\varphi_h^n)\|_{L^\infty(\Omega)}\le\frac{\varepsilon_1^n}{\varepsilon}, \tag{5.7}$$

and

$$\|T(\varphi(.,t_n)) - T(\varphi_h^n)\|_{L^2(\Omega)^{d\times d}} \le c\,\big(\frac{\varepsilon_1^n}{\varepsilon^2} + \frac{\varepsilon_2^n}{\varepsilon}\big). \tag{5.8}$$

Proof. The two estimates in (5.7) come from the fact that H_ε is Lipschitz-continuous (the norm of its derivative is bounded by $\frac{1}{\varepsilon}$). To prove (5.8), we use the triangle inequality

$$\begin{aligned}
&\|T(\varphi(.,t_n)) - T(\varphi_h^n)\|_{L^2(\Omega)^{d\times d}} \\
&\quad\le \|\sigma\big(\frac{dH_\varepsilon(\varphi(\cdot,t_n))}{d\varphi} - \frac{dH_\varepsilon(\varphi_h^n)}{d\varphi}\big)(I - \nabla\varphi\otimes\nabla\varphi)(\cdot,t_n)\|_{L^2(\Omega)^{d\times d}} \\
&\qquad + \|\sigma\frac{dH_\varepsilon(\varphi_h^n)}{d\varphi}(\nabla(\varphi(\cdot,t_n) - \varphi_h^n)\otimes\nabla\varphi(\cdot,t_n))\|_{L^2(\Omega)^{d\times d}} \\
&\qquad\quad + \|\sigma\frac{dH_\varepsilon(\varphi_h^n)}{d\varphi}(\nabla\varphi(\cdot,t_n)\otimes\nabla(\varphi(\cdot,t_n) - \varphi_h^n))\|_{L^2(\Omega)^{d\times d}} \\
&\qquad\qquad + \|\sigma\frac{dH_\varepsilon(\varphi_h^n)}{d\varphi}(\nabla(\varphi(\cdot,t_n) - \varphi_h^n))\otimes\nabla(\varphi(\cdot,t_n) - \varphi_h^n))\|_{L^2(\Omega)^{d\times d}}.
\end{aligned}$$

We observe that $\frac{dH_\varepsilon}{d\varphi}$ is also Lipschitz-continuous, with bounded Lipschitz constant (by $\frac{\pi}{2\varepsilon^2}$). We use Proposition 5.2 for the first term, Proposition 5.3 (with $p = 4$ for instance) for the last three terms, and obtain the desired result.

To go further, we subtract the first line of (4.9) from the first line of equation (3.7) at time t_n, which gives for any $\boldsymbol{v}$ in $\mathbb{X}_h^n$,

$$\begin{aligned}
&\int_\Omega \Big(\rho(\varphi)(\boldsymbol{x},t_n)\big(\frac{\partial\boldsymbol{u}}{\partial t} + \boldsymbol{u}\cdot\nabla\boldsymbol{u}\big)(\boldsymbol{x},t_n) - \rho(\varphi_h^n)(\boldsymbol{x})\big(\frac{\boldsymbol{u}_h^n - \tilde{\boldsymbol{u}}_h^{n-1}}{\tau_n}\big)(\boldsymbol{x})\Big)\boldsymbol{v}(\boldsymbol{x})\,d\boldsymbol{x} \\
&\quad - \int_\Omega (\nabla\cdot\boldsymbol{v})(\boldsymbol{x})\big(p(\boldsymbol{x},t_n) - p_h^n(\boldsymbol{x})\big)\,d\boldsymbol{x} \\
&\qquad + \int_\Omega \Big(\nu(\varphi)(\boldsymbol{x},t_n)\nabla\boldsymbol{u}(\boldsymbol{x},t_n) - \nu(\varphi_h^n)(\boldsymbol{x})\nabla\boldsymbol{u}_h^n(\boldsymbol{x})\Big) : \nabla\boldsymbol{v}(\boldsymbol{x})\,d\boldsymbol{x} \\
&\qquad\quad = \int_\Omega \big(T(\varphi(\boldsymbol{x},t_n)) - T(\varphi_h^n)(\boldsymbol{x})\big) : \nabla\boldsymbol{v}(\boldsymbol{x})\,d\boldsymbol{x}.
\end{aligned} \tag{5.9}$$

The key idea consists in inserting in this equation the mean value

$$M_n(\boldsymbol{x}) = \frac{1}{\tau_n}\int_{t_{n-1}}^{t_n} \big(\frac{\partial\boldsymbol{u}}{\partial t} + \boldsymbol{u}\cdot\nabla\boldsymbol{u}\big)(\boldsymbol{x},t)\,dt.$$

Indeed, it is equal to

$$M_n(\boldsymbol{x}) = \frac{\boldsymbol{u}(\boldsymbol{x},t_n) - \boldsymbol{u}(X(\boldsymbol{x},t_n;t_{n-1}))}{\tau_n},$$

thus easier to compare to the discrete one, and standard arguments yield that, if $\boldsymbol{u}$ belongs to $H^2(t_{n-1},t_n;L^2(\Omega)^d)$ and C_n denotes its norm in this space

$$\|\big(\frac{\partial\boldsymbol{u}}{\partial t} + \boldsymbol{u}\cdot\nabla\boldsymbol{u}\big)(\cdot,t_n) - M_n\|_{L^2(\Omega)^d} \le C_n\tau_n. \tag{5.10}$$

From now on and for simplicity, we forget the dependency of the estimates with respect to ε (so that the righthand side of estimate (5.8) reads $c\,\varepsilon_2^n$).

Proposition 5.5. *Assume that the solution φ of problem* (3.3) *satisfies* (5.3) *and that the solution $(\boldsymbol{u}, p)$ of problem* (3.6) − (3.7) *is such that*

$$\begin{aligned} \boldsymbol{u} \in W^{1,\infty}(\Omega\times]0,T_f[) \cap H^2(0,T_f;L^2(\Omega)^d) \cap L^\infty(0,T_f;H^2(\Omega)^d), \\ p \in L^\infty(0,T_f;H^2(\Omega)). \end{aligned} \tag{5.11}$$

Then, the following estimate holds for $1 \le n \le N$

$$\tau_n^{-1}\|\boldsymbol{u}(\cdot,t_n) - \boldsymbol{u}_h^n\|_{L^2(\Omega)^d} + |\boldsymbol{u}(\cdot,t_n) - \boldsymbol{u}_h^n|_{H^1(\Omega)^d} \le C\,(h_n + \tau_n) + c\,\varepsilon_2^n, \tag{5.12}$$

where the constant C only depends on the regularity of φ, $\boldsymbol{u}$ and p.

Proof. Since many terms in (5.9) have already been evaluated, we present it in an abridged way. In (5.9), we add and subtract $\mathcal{I}_h^n\boldsymbol{u}$ in the first terms and take $\boldsymbol{v}$ equal to $\mathcal{I}_h^n\boldsymbol{u}(\cdot,t_n) - \boldsymbol{u}_h^n$. We observe from the second equations of (3.7) and (4.9) that the term involving the pressure can be written as

$$\begin{aligned} &-\int_\Omega \big(\nabla\cdot(\mathcal{I}_h^n\boldsymbol{u}(\cdot,t_n) - \boldsymbol{u}_h^n)\big)(\boldsymbol{x})\big(p(\boldsymbol{x},t_n) - p_h^n(\boldsymbol{x})\big)\,d\boldsymbol{x} \\ &= \int_\Omega \big(\nabla\cdot(\boldsymbol{u} - \mathcal{I}_h^n\boldsymbol{u})(\cdot,t_n)\big)(\boldsymbol{x})\big(p(\boldsymbol{x},t_n) - p_h^n(\boldsymbol{x})\big)\,d\boldsymbol{x} + \int_\Omega \big(\nabla\cdot\boldsymbol{u}_h^n\big)(\boldsymbol{x})(p - \mathcal{I}_h^n p)(\boldsymbol{x},t_n)\,d\boldsymbol{x}, \end{aligned}$$

and we integrate by parts the first term.
All this leads to a bound of the quantity

$$\tau_n^{-1}\|\mathcal{I}_h^n\boldsymbol{u}(\cdot,t_n) - \boldsymbol{u}_h^n\|^2_{L^2(\Omega)^d} + |\mathcal{I}_h^n\boldsymbol{u}(\cdot,t_n) - \boldsymbol{u}_h^n|^2_{H^1(\Omega)^d}$$

by terms either evaluated in Lemma 5.4 or in (5.10) or involving interpolation error. We conclude by using triangle inequalities and interpolation estimates.

Remark 5.6. Owing to the inf-sup condition (4.12), an error estimate for the pressure $p(\cdot,t_n) - p_h^n$ can also be derived, we skip it for brevity.

Unfortunately, the term ε_2^n contains error terms at time t_{n-1}, so we need an induction on n to conclude. We denote by h the maximum of the h_n, $0 \le n \le N$.

Theorem 5.7. *Assume that the solution $(\varphi, \boldsymbol{u}, p)$ of problem* (3.3) − (3.6) − (3.7) *is such that*

$$\begin{aligned} &\varphi \in \mathscr{C}^0(0,T_f;W^{2,\infty}(\Omega)), \\ &\qquad \boldsymbol{u} \in W^{1,\infty}(\Omega\times]0,T_f[) \cap H^2(0,T_f;L^2(\Omega)^d) \cap \mathscr{C}^0(0,T_f;H^2(\Omega)^d), \\ &\qquad\qquad p \in L^\infty(0,T_f;H^2(\Omega)). \end{aligned} \tag{5.13}$$

For $1 \le n \le N$, let us choose the parameters τ and h such that,

$$h \le c\,h_{n,\min}, \qquad |\tau| \le c\,h_{n,\min}^2. \tag{5.14}$$

Then, the following estimates hold for $1 \leq n \leq N$

$$\|\varphi(\cdot, t_n) - \varphi_h^n\|_{L^\infty(\Omega)} \leq C_n\,(h^2 + |\tau|), \tag{5.15}$$

and

$$\|\boldsymbol{u}(\cdot, t_n) - \boldsymbol{u}_h^n\|_{H^1(\Omega)^d} \leq C_n\,(h + |\tau|), \tag{5.16}$$

where the constant C_n *depends on the regularity of* φ, $\boldsymbol{u}$ *and* p, *and also on* n.

Proof. We proceed by induction on n.
1) For $n = 0$, estimates (5.15) and (5.16) are obvious since φ_h^0 and $\boldsymbol{u}_h^0$ are the interpolates of φ_0 and $\boldsymbol{u}_0$, respectively.
2) Assume that (5.15) and (5.16) hold for $n-1$. We use the inverse inequality (with $\eta > 0$)

$$\begin{aligned}\|\boldsymbol{u}_h^{n-1}\|_{L^\infty(\Omega)^d} \leq\ & \|\boldsymbol{w}_h\|_{L^\infty(\Omega)^d} \\ & + h_{n-1,\min}^{1-\frac{d}{2}-\eta}(\|\boldsymbol{u}(\cdot, t_{n-1}) - \boldsymbol{w}_h\|_{H^1(\Omega)^d} + \|\boldsymbol{u}(\cdot, t_{n-1}) - \boldsymbol{u}_h^{n-1}\|_{H^1(\Omega)^d}),\end{aligned}$$

where $\boldsymbol{w}_h$ is any approximation of $\boldsymbol{u}(\cdot, t_{n-1})$ in $\mathbb{X}_h^{n-1}$, and thus we derive from (5.14) and the induction hypothesis that $\|\boldsymbol{u}_h^{n-1}\|_{L^\infty(\Omega)^d}$ is bounded. Then, inserting the induction hypothesis in (5.4) and (5.12) gives (5.15) and (5.16), respectively.

Despite the technicity of the proofs, estimates (5.15) and (5.16) are fully optimal. But condition (5.14) is too restrictive: it involves both a hard Courant–Friedrichs–Lévy condition and the uniform regularity of the families of triangulations. Fortunately the same arguments as in the previous proof lead to the following result.

Corollary 5.8. *Assume that the solution* $(\varphi, \boldsymbol{u}, p)$ *of problem* $(3.3) - (3.6) - (3.7)$ *satisfies* (5.13). *For* $1 \leq n \leq N$, *let us choose the parameters* τ *and* h *such that, for a positive constant* η,

$$h^2 + |\tau| \leq c\, h_{n,\min}^{\frac{d}{2}+\eta}. \tag{5.17}$$

Then, the following estimates hold for $1 \leq n \leq N$

$$\|\varphi(\cdot, t_n) - \varphi_h^n\|_{L^\infty(\Omega)} \leq C_n\,(h^2 + |\tau|), \tag{5.18}$$

and

$$\|\boldsymbol{u}(\cdot, t_n) - \boldsymbol{u}_h^n\|_{H^1(\Omega)^d} \leq C_n\, h_{n,\min}^{-1}(h^2 + |\tau|), \tag{5.19}$$

where the constant C_n *depends on the regularity of* φ, $\boldsymbol{u}$ *and* p, *and also on* n.

Assumption (5.17) is much more realistic and the convergence of the discretization holds for standard properties of the family of triangulations.

Remark 5.9. The fact that the constant C_n in estimates (5.15), (5.16), (5.18) and (5.19) depends on n can be avoided either by weakly strengthening conditions (5.14) and (5.17) or working with specific family of parameters: for instance, it can be assumed that the quantity $h_n^2 + \tau_n$ decreases with n.

Remark 5.10. We refer to [3] for a detailed a posteriori analysis of the method of characteristics. Since the same arguments hold for our discretization, we have decided not to perform the a posteriori analysis of problem $(4.4) - (4.5) - (4.6) - (4.9)$.

6. Numerical results.

In the absence of analytical solutions, which are very hard to come by for this model, its validation is best accomplished with numerical benchmarking. In this section, we present three well-known test problems for the computation of two immiscible fluids with surface tension. All the examples are described in two dimensions and using FreeFem++ software, see [15]. The level set method is applied to solve them with the ability to capture the changes of the topology correctly. So, the interface is captured by level set function which is defined as a signed distance function described in Section 2. Note that, all computations are performed using:

- the symmetric operator $\nabla \cdot (\nu(\nabla \boldsymbol{u} + \nabla \boldsymbol{u}^t))$ in the Navier-Stokes equation,
- the characteristics method with fixed time step,
- the parameter g denotes the gravitational acceleration.

6.1. Rayleigh–Taylor instability.

The widely used test problem for numerical simulations for two-fluid flow is the Rayleigh–Taylor instability, see for instance [32]. When a layer of heavier fluid is placed on top of another lighter layer in a gravitational field with gravity pointing downward, the initial planar interface is unstable. Any disturbance will grow to produce spikes of heavier fluid moving downwards and bubbles of lighter fluid moving upwards. This is the so-called Rayleigh–Taylor instability. In this test case a heavy fluid is placed on the top of a light fluid and the initial position of the perturbed interface between two fluids is

$$\varphi(\boldsymbol{x}) = \tanh \frac{y - 2 - 0.1\cos(2\pi\, x)}{0.01\sqrt{2}}$$

The computational domain is the rectangle $]0, a[\times]0, 4a[$ where $a = 1$ is the width. The density difference is normally represented by the Atwood number

$$At = \frac{\rho_2 - \rho_1}{\rho_2 + \rho_1},$$

where $\rho_2 > \rho_1$ correspond to the heavier and lighter fluids, respectively. We also introduce the following Reynolds number

$$Re = \frac{\rho_1 a^{\frac{3}{2}} g^{\frac{1}{2}}}{\nu}.$$

According to [32], the governing equations are made dimensionless by using the following references: $\rho_{ref} = \rho_1$, $a_{ref} = a$ and $t_{ref} = t\sqrt{a\, At\, g}$. A no-slip condition $\boldsymbol{u} = (0, 0)$ is enforced at the bottom and top walls while the first component of velocity $u_1 = 0$ is imposed on the two vertical sides, and we work with $\varepsilon = 0.05$. The interface shape at different dimensional times (for instance, $t = 0s, 1s, 2s, 3s, 4s$) are plotted in Figure 2 and Figure 3. In the first one, the Reynolds number Re is equal to 100 and the Atwood number is equal to $At = 0.3$, while in the second one we take $Re = 1000$ and $At = 0.5$. During the

early stages, the growth of the interface is slow and remains symmetrical. However, the characteristic mushroom shape emerges in the vicinity of the central vortex. Later, the heavier fluid falls continuously and the lighter fluid keep rising to form bubbles along the vertical side boundary, and the heavier fluid begins to roll up into two counter-rotating vortices.

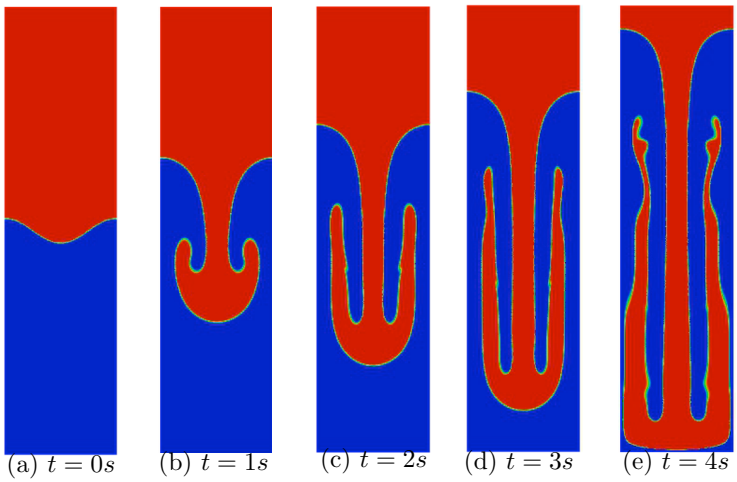

(a) $t = 0s$ (b) $t = 1s$ (c) $t = 2s$ (d) $t = 3s$ (e) $t = 4s$

Figure 2. Rayleigh-Taylor instability.

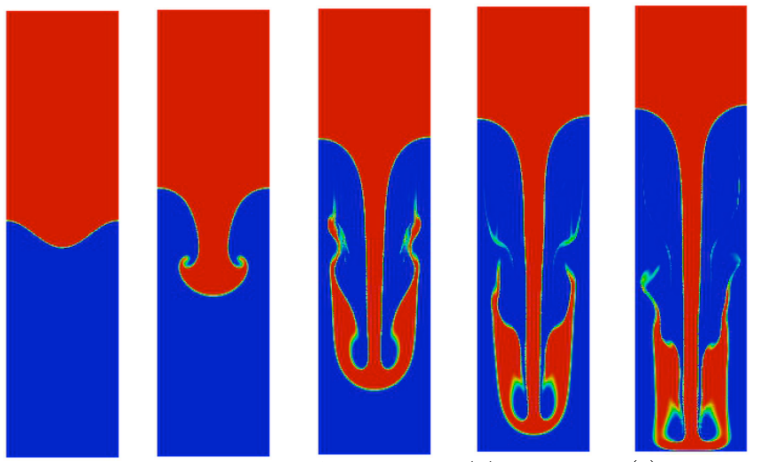

(a) $t = 0s$ (b) $t = 1s$ (c) $t = 1.2s$ (d) $t = 1.75s$ (e) $t = 2.25s$

Figure 3. Rayleigh-Taylor instability.
$At = 0.5$ and $Re = 1000$: evolution of the interface shape in time

Finally, in order to study the effect of the Atwood number, we fixe the Reynolds number at $Re = 1000$ and we increase the Atwood number: $At = 0.3, 0.35, 0.4, 0.45$ and $At = 0.5$. It can easily be seen in Figure 4 or Figure 5 that with increasing Atwood number

the mushroom is more roll up.

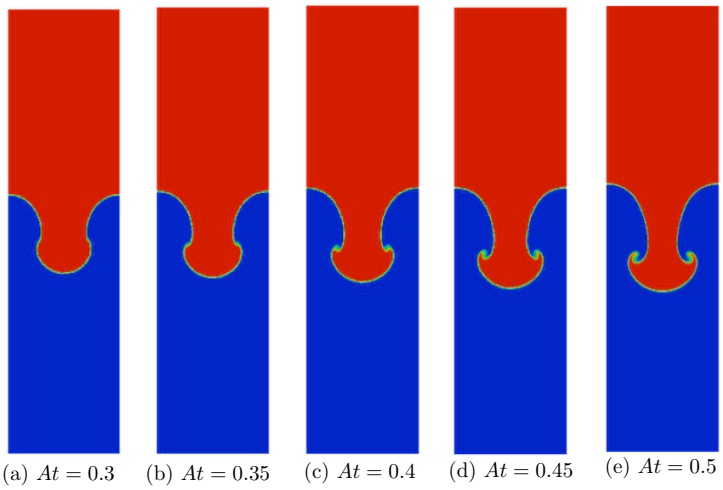

Figure 4. Rayleigh-Taylor instability.
$Re = 1000$: evolution of the interface shape with respect to At

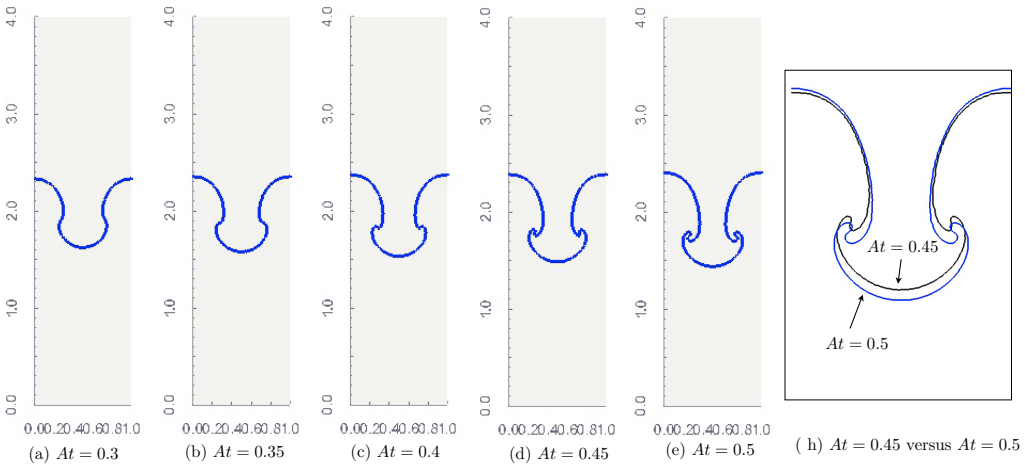

Figure 5. Rayleigh-Taylor instability.
$Re = 1000$: evolution of the interface shape with respect to At

6.2. Two-dimensional rising bubble.

The next application is a circular bubble rising in a viscous fluid. For this simulation, we use data from the numerical experiment of Hysing et al. [18] where the bubble is initially circular with radius $r = 0.25$ and center coordinates $(0.5, 0.5)$ placed at the bottom of a rectangular domain $]0, 1[\times]0, 2[$ with another fluid of higher density and viscosity. Figure 6 illustrates the initial configuration of this problem and the boundary conditions we use.

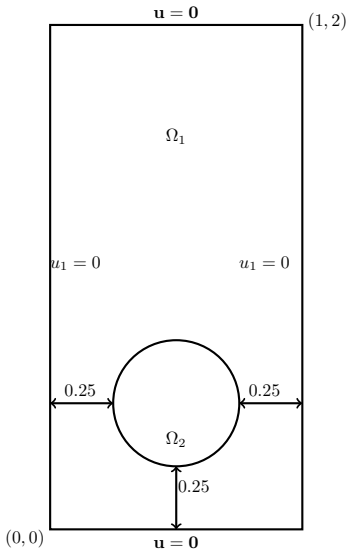

Figure 6. Rising bubble: boundary condition and initial configuration

The parameter ε is taken equal to 0.025. Buoyancy effects will make the drop move to the top of the domain and undergo some deformation. The result shape depends naturally on different physical parameters, for instance on Reynolds number $Re = \dfrac{2r\rho_1\sqrt{2rg}}{\nu_1}$ and on the so-called Eötvös number which gives the ratio of gravitational forces to surface tension effects $Eo = \dfrac{4r^2 g\rho_1}{\sigma}$. The density and viscosity of the heavy fluid are ρ_1, ν_1 whereas density and viscosity of the fluid occupied by the bubble are ρ_2, ν_2. In order to compare our results to the benchmark performed in [18], we decide to realize two test cases: the first one considers a bubble with small density and viscosity ratios = 10, which undergoes moderate shape deformation and for the second test case, a bubble with a very low density and viscosity, where the ratios are 1000 (resp. 100) compared to that of the surrounding fluid.

• **Test case 1:** $\rho_1 = 1000, \rho_2 = 100, \nu_1 = 10, \nu_2 = 1, \sigma = 24.5$ and $g = 0.98$. Thus $Re = 35$ and $Eo = 10$.

• **Test case 2:** $\rho_1 = 1000, \rho_2 = 1, \nu_1 = 10, \nu_2 = 0.1, \sigma = 1.96$ and $g = 0.98$. This yields $Re = 35$ and $Eo = 125$.

Subsequently, we introduce the following quantities allowing the quantitative comparison

with Hysing et al. results [18]: the centroid or center of mass in order to track the translation of bubble $(x_c, y_c)(t) = \int_{\Omega_2} \boldsymbol{x} d\boldsymbol{x} / \int_{\Omega_2} d\boldsymbol{x}$, and the rise velocity $u_2(x_c, y_c; t)$ which is the velocity component in the direction opposite to the gravitational vector. For both test cases, we use the mesh adaptation in order to capture efficiently the interface between flows.

Test case 1 results:

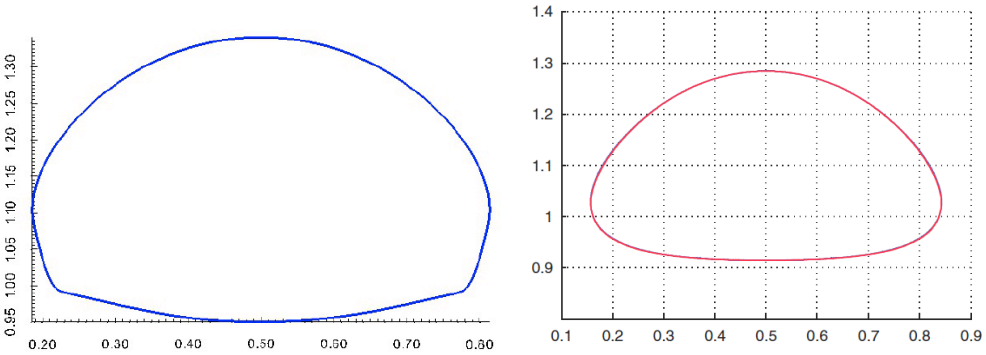

Figure 7. Bubble shape at the final time ($t = 3$) for the test case 1. Left: Our result. Right: Hysing et al.

Figures 7 shows both shapes obtained by our simulation in the left panel and by Hysing et al. in the right side. They have a similar form and we observe that the maximum of width and the height have almost the same values. Furthermore, Figure 8 confirms quantitatively that the rise velocity and the centre of mass are identical:

- the maximum rise velocity has an approximate magnitude of 0.24 and occurs between times $t = 0.9$ and $t = 0.94$
- the evolution of the center of mass can be described as a linear function of time and approaches $y_c = 1.09$ toward the end of both simulations.

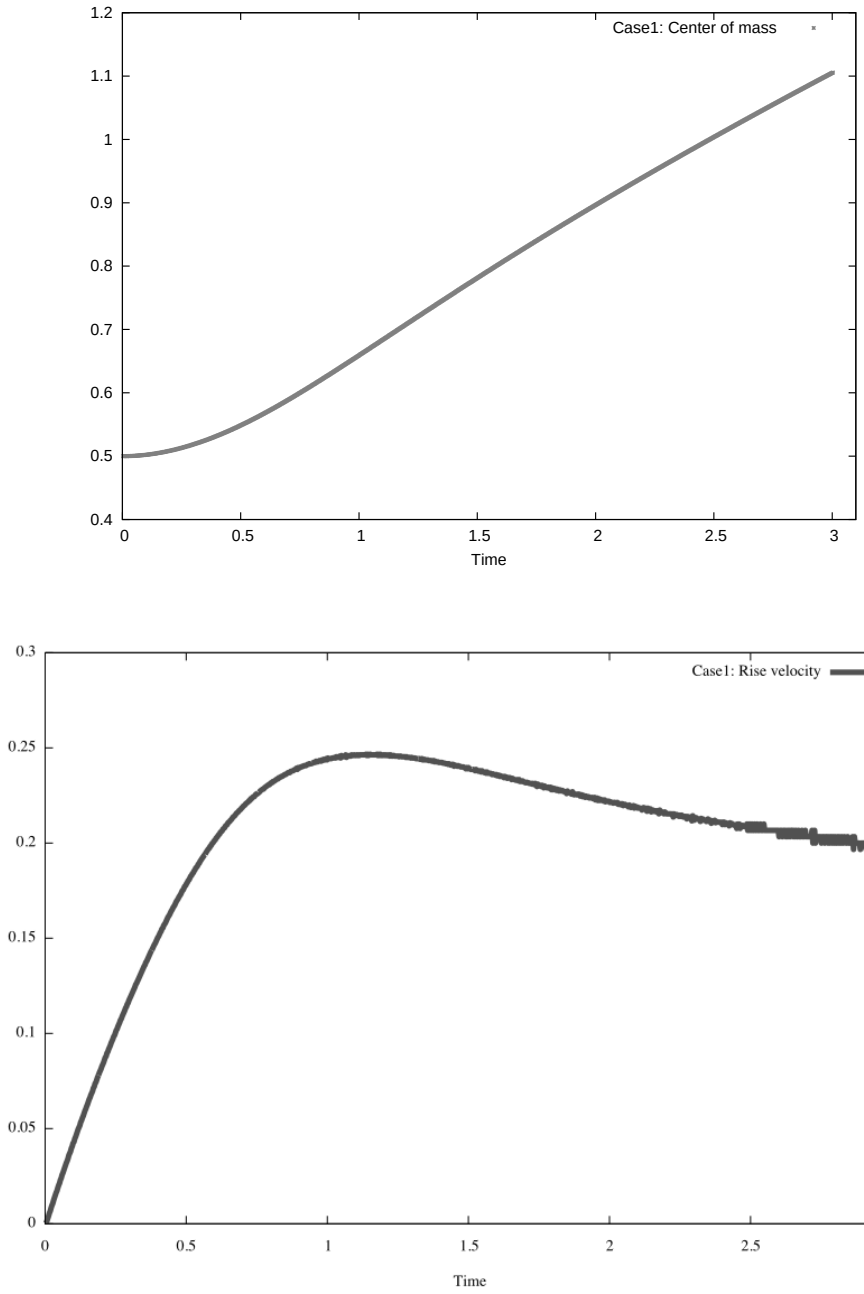

Figure 8. Our work: Center of mass (top) and rise velocity (bottom) for test case 1

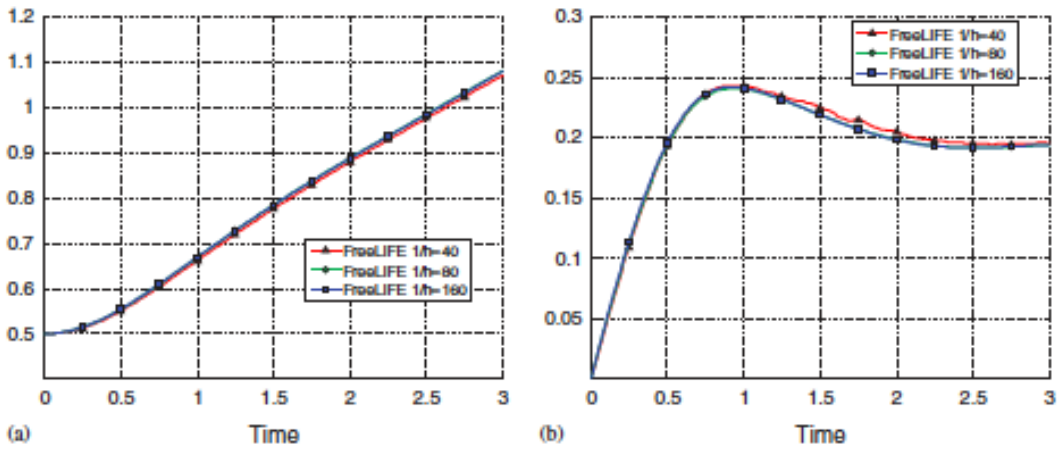

Figure 9. Bubble shape at the final time ($t = 3$) for the test case 1. Left: Our result. Right: Hysing et al.

Test case 2 results:

As mentioned above, in the test case 2 , we increase the Eötvös number to $Eo = 125$. Figures 10 and 11 describe the evolution in time of the shape deformation obtained in this work and in [18]. So, we can observe that under $t = 2.2$ (the top panel of Figures 10 and 11), the results are similar.

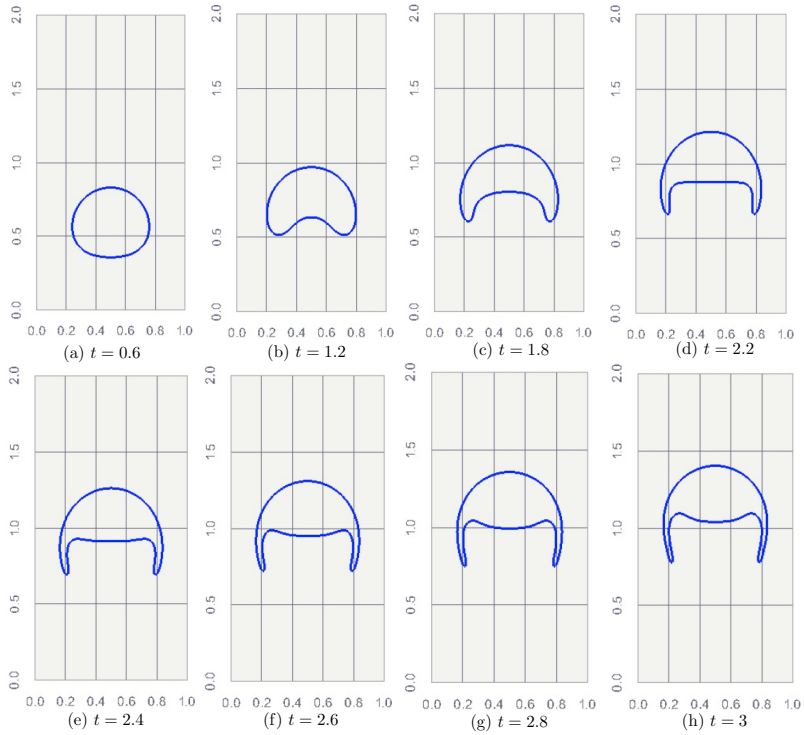

Figure 10. Our result: Typical time evolution of the interface for test case 2

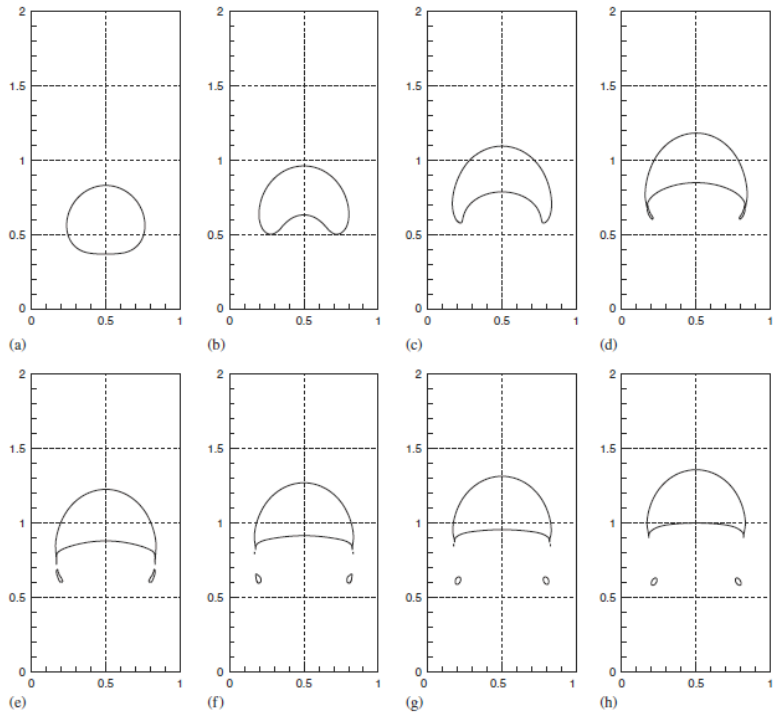

Figure 11. Hysing et al.: Typical time evolution of the interface for test case 2

However, in the bottom side of Figures 10 and 11, i.e $t > 2.2$, the behavior of the shapes are different. The small satellite droplets trail the bulk of the main bubble in the work of Hysing et al. We think that the mesh adaptation is necessary to avoid this problem. Figure 12 shows all meshes during the computation.

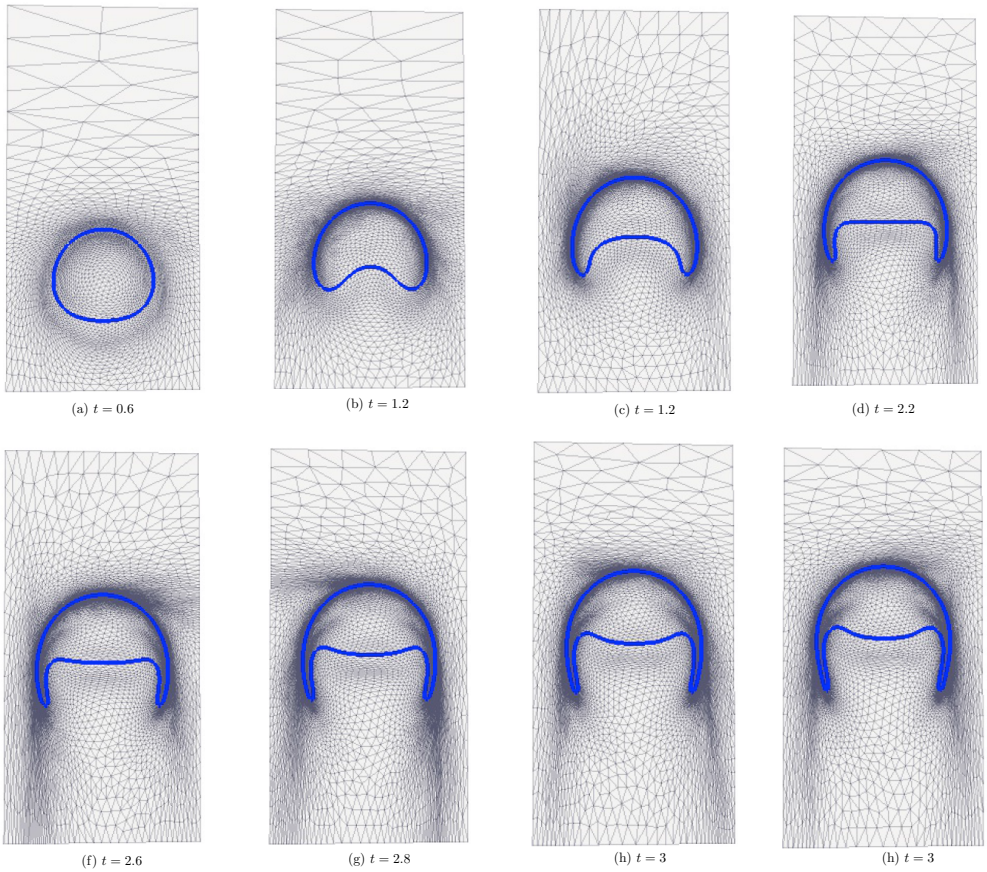

Figure 12. Our result: Typical time evolution of the adaptive mesh for test case 2

Nevertheless, the center of mass of both simulations is similar, see Figures 13 and 14. Concerning the maximum rise velocity, the results in [18] shows that there exist two velocity maxima, the first occurring at time $t = 0.7332$ with a magnitude of 0.2524 and the second one at $t = 2.0705$ with a slightly smaller magnitude of 0.2434, see the right side of Figure 12. Whereas in our work, Figure 13 (right side) shows two velocity maxima. The first is obtained at time ≈ 0.7 with a magnitude ≈ 0.25. But, the maximum of the second rise velocity is close to 0.24 at time $t \approx 1.7$.

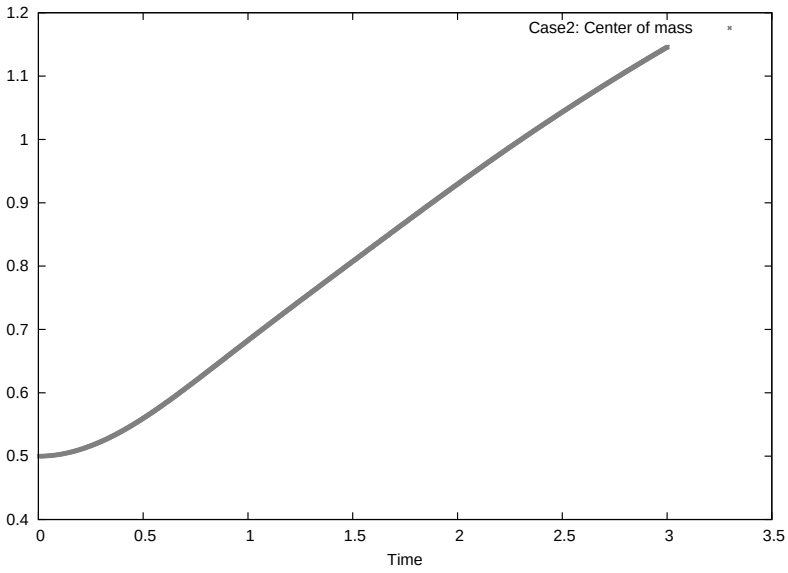

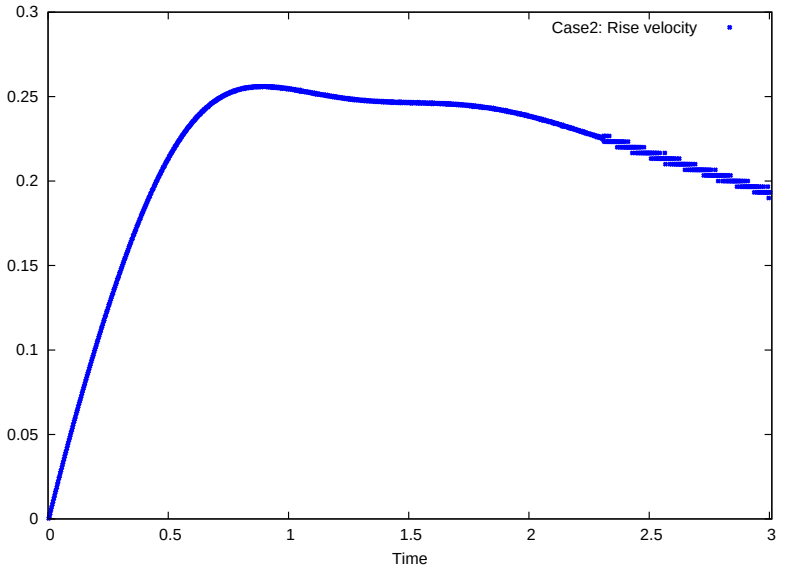

Figure 13. Our work: Center of mass (top) and rise velocity (bottom) for test case 2

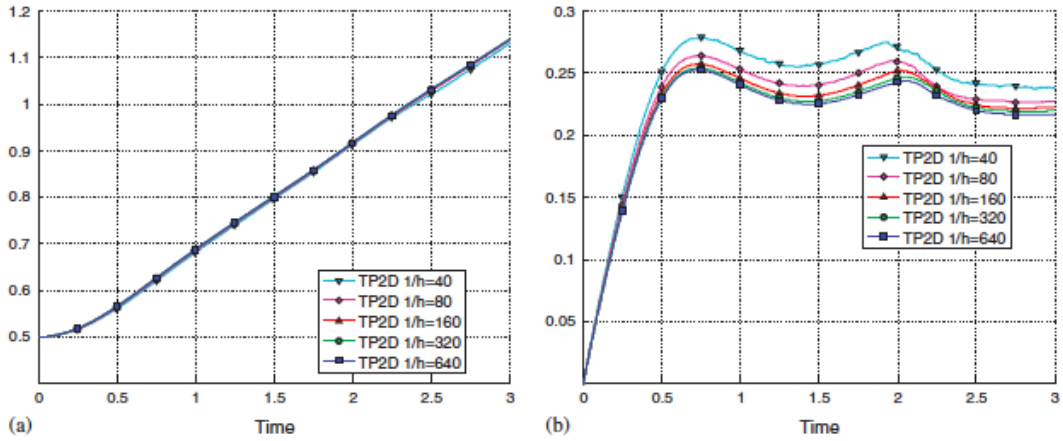

Figure 14. Hysing et al.: Center of mass (left) and rise velocity (right) for test case 2

6.3. Interstitial fluid in a jogged channel.

We present in this section a numerical simulation of the evolution of a bubble in a so-called *jogged* channel. The parameter ε is now taken equal to 0.05. The viscosities and densities of the external (resp. internal) fluid are $\nu_1 = 1, \nu_2 = 0.1$ and $\rho_1 = 100, \rho_2 = 1$.

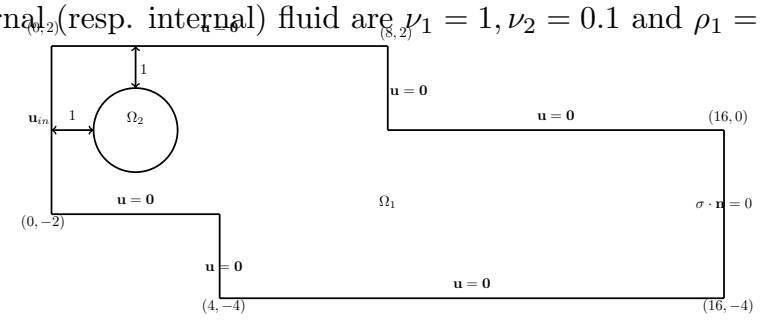

Figure 15. Boundary condition and initial configuration

This test is mentioned shortly by Chessa et al. in [8], and we are going to try to complete this study by varying the surface tension coefficient σ and then plotting the shape deformation, the center of mass (x_c, y_c) (as in the above example) and both velocity components $u_1(x_c, y_c)$, $u_2(x_c, y_c)$. The initial droplet shape has a largest diameter 2, as shown in Figure 15. During time, the droplet changes its shape and then translate from left to right in the jogged channel without gravitational effects. An the inlet (left wall), the Poiseuille flow $\boldsymbol{u} = \boldsymbol{u}_{in} = \left(\frac{(2-y)\,(y+2)}{4}, 0\right)$ is assigned and the natural Neumann condition

$$\sigma \cdot \boldsymbol{n} = \nu(\nabla \boldsymbol{u} + \nabla \boldsymbol{u}^t) \cdot \boldsymbol{n} + p\,\boldsymbol{n} = 0$$

is imposed in the outlet (right wall). All boundary conditions are explained in Figure 15.

The parameter ε is fixed equal to 0.05. At each step, the mesh adaptation is used in order to capture the interface nicely and the time step is taken constant equal to $4 \cdot 10^{-2}$.

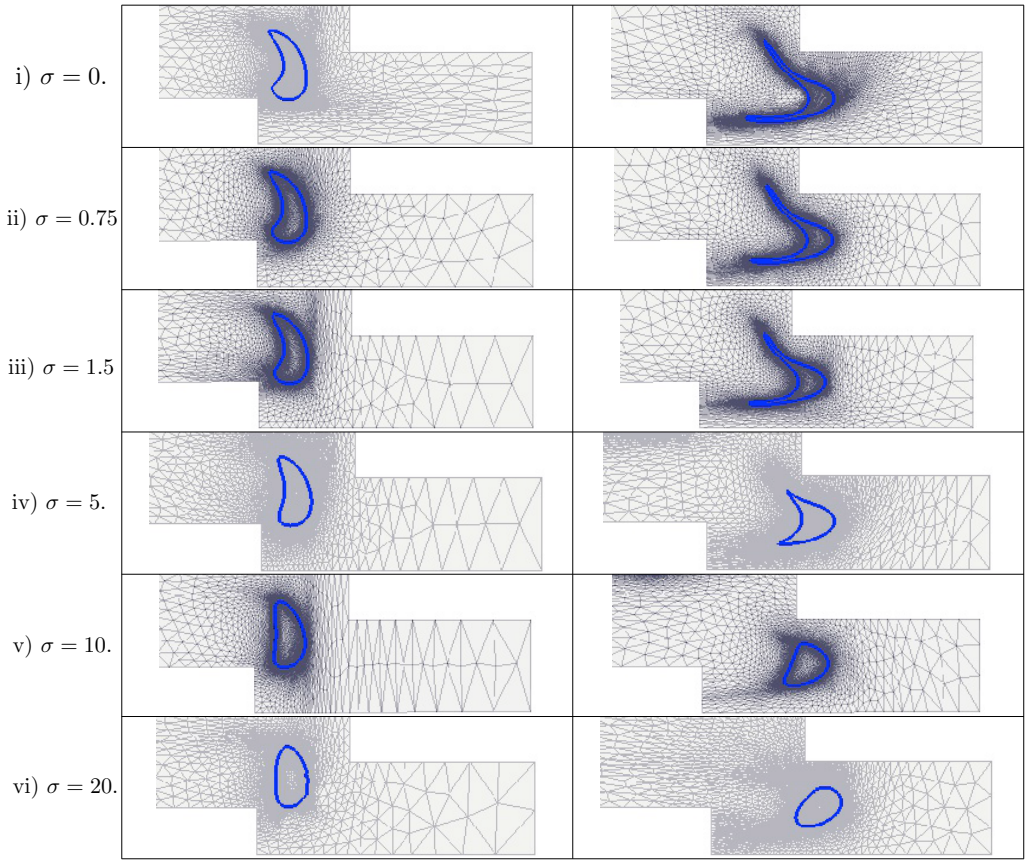

Figure 16. Time evolution of the shape and meshes with respect to the surface tension coefficient σ

Figure 16 shows the time evolution of the deformation of the bubble with respect to the tension surface coefficient σ. We observe that when σ increases from $\sigma = 0$ to $\sigma = 20$, the shape deformation of the bubble decreases and we remark that the shapes for the small $\sigma = 0.75$ and 1.5 have the same geometries. However, for $\sigma = 5, 10$ or 20, all results are different especialy when $t = 8$.

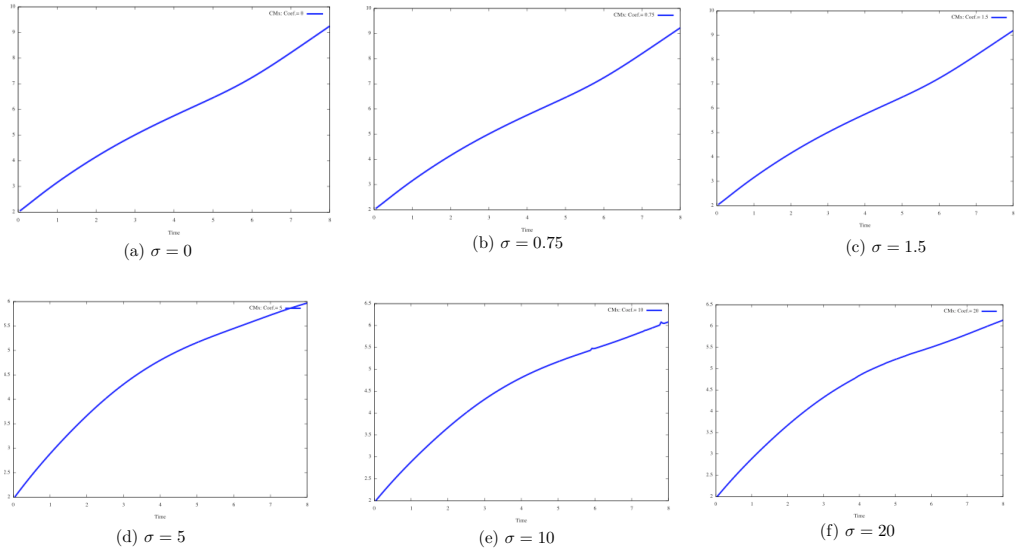

(a) $\sigma = 0$ (b) $\sigma = 0.75$ (c) $\sigma = 1.5$

(d) $\sigma = 5$ (e) $\sigma = 10$ (f) $\sigma = 20$

Figure 17. Center of mass x_c with respect surface tension coefficient σ

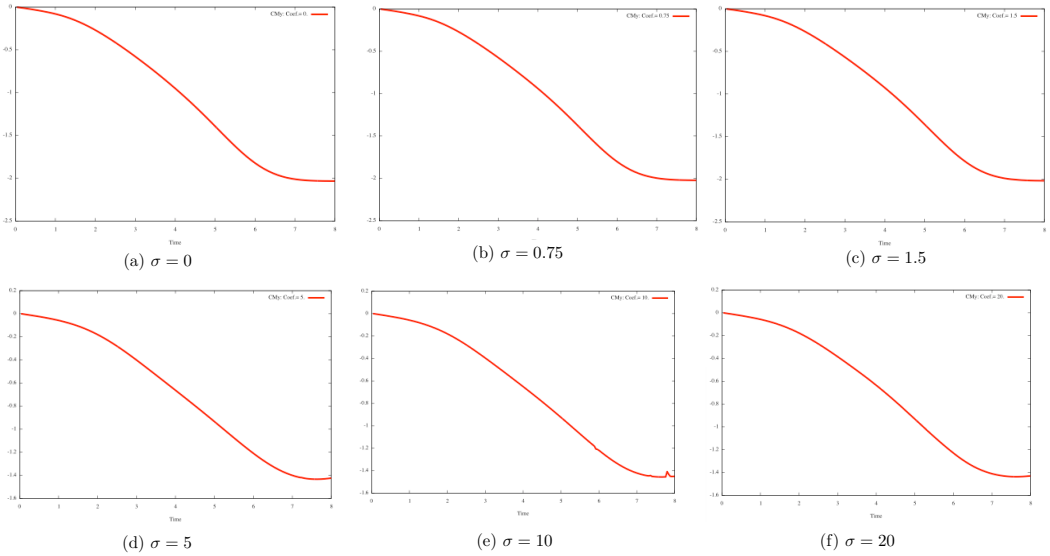

(a) $\sigma = 0$ (b) $\sigma = 0.75$ (c) $\sigma = 1.5$

(d) $\sigma = 5$ (e) $\sigma = 10$ (f) $\sigma = 20$

Figure 18. Center of mass y_c with respect surface tension coefficient σ

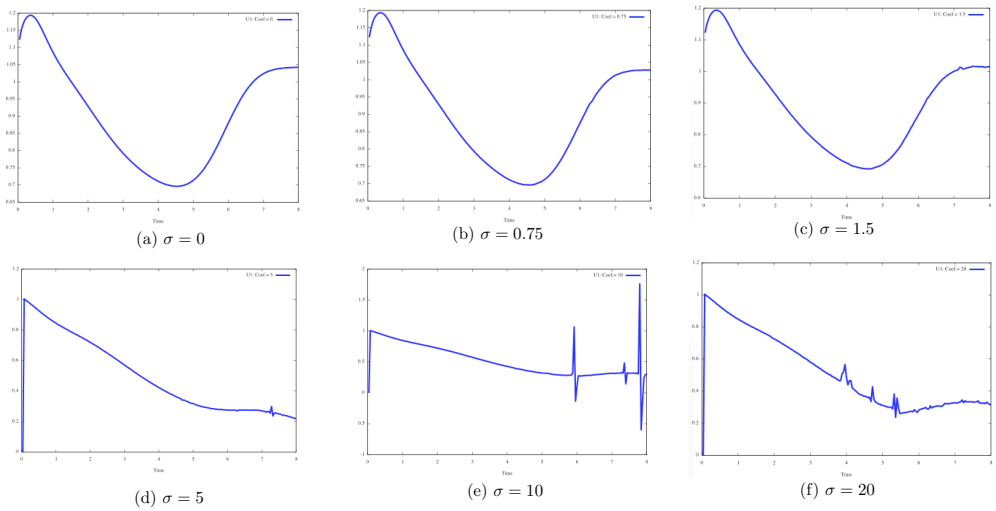

(a) $\sigma = 0$ (b) $\sigma = 0.75$ (c) $\sigma = 1.5$

(d) $\sigma = 5$ (e) $\sigma = 10$ (f) $\sigma = 20$

Figure 19. Velocity $u_1(x_c, y_c)$ with respect surface tension coefficient σ

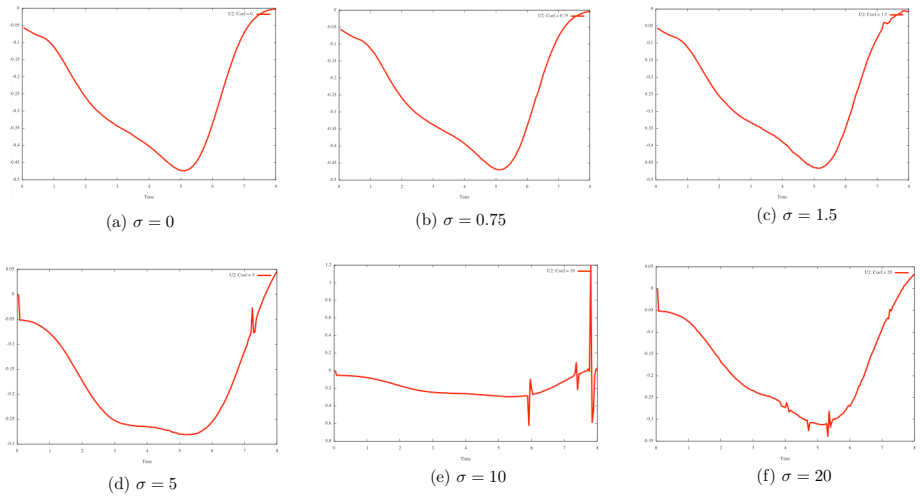

(a) $\sigma = 0$ (b) $\sigma = 0.75$ (c) $\sigma = 1.5$

(d) $\sigma = 5$ (e) $\sigma = 10$ (f) $\sigma = 20$

Figure 20. Velocity $u_2(x_c, y_c)$ with respect surface tension coefficient σ

Concerning the center of mass and velocities, Figures 18 to 20 confirm the previous remarks.

References

[1] R.A. Adams, J. Fournier — *Sobolev Spaces*, Academic Press (2003).

[2] H. Amann — *Ordinary differential equations*, de Gruyter Studies in Mathematics, vol. 13, Walter de Gruyter & Co., Berlin, 1990, An introduction to non-linear analysis, Translated from the German by Gerhard Metzen.

[3] C. Bernardi, F. Hecht, R. Verfürth — A posteriori error analysis of the method of characteristics, *Math. Models and Methods in Applied Sciences* **21** (2011), 1355–1376.

[4] C. Bernardi, Y. Maday, F. Rapetti — *Discrétisations variationnelles de problèmes aux limites elliptiques*, Collection "Mathématiques et Applications" **45**, Springer-Verlag (2004).

[5] K. Boukir, Y. Maday, B. Métivet, E. Razafindrakoto — A high-order characteristics/finite element method for the incompressible Navier-Stokes equations, *Int. J. Numer. Meth. Fluids* **25** (1997), 1421–1454.

[6] F. Boyer, P. Fabrie — *Mathematical Tools for the Study of the Incompressible Navier-Stokes Equations and Related Models*, Applied Mathematical Sciences; Vol. 183, Springer (2013).

[7] J.U. Braekbill, D.B. Kothe, C. Zemach — A continuum method for modeling surface tension, *J. Comput. Physics* **100** (1992), 335–383.

[8] J. Chessa, T. Belytschko — An extended finite element method for two-phase fluids, *Journal of Applied Mechanics* **70** (2003), 10–17.

[9] G.-H. Cottet, E. Maitre, T. Milcent — Eulerian formulation and level set models for incompressible fluid-structure interaction, *Math. Model. Numer. Anal.* **42** (2008), 471–492.

[10] R.J. DiPerna, P.L. Lions — Ordinary differential equations, transport theory and Sobolev spaces, *Invent. Math.* **98** (1989), 511–547.

[11] V. Doyeux, Y. Guyot, V. Chabannes, C. Prud'Homme, M. Ismail — Simulation of two-fluid flows using a finite element/level set method. Application to bubbles and vesicle dynamics, *Journal of Computational and Applied Mathematics* **246** (2013), 251–259.

[12] P. Frey, T.T.M. Ta — A numerical scheme based on level set method and anisotropic mesh adaptation for solving two-fluid flows, *Int. J. Numer. Meth. Fluids* (2013), 1–28.

[13] V. Girault, P.-A. Raviart — *Finite Element Approximation of the Navier–Stokes Equations*, Lecture Notes in Mathematics **749**, Springer–Verlag (1979).

[14] V. Girault, P.-A. Raviart — *Finite Element Methods for Navier–Stokes Equations, Theory and Algorithms*, Springer–Verlag (1986).

[15] F. Hecht — New development in FreeFem++, *Journal of Numerical Mathematics* **20** (2012), 251–266.

[16] P. Hood, C. Taylor — A numerical solution of the Navier–Stokes equations using the finite element technique, *Comp. and Fluids* **1** (1973), 73–100.

[17] T.Y. Hou, J.S Lowengrub, M.J. Shelley — Boundary integral methods for multicomponent fluids and multiphase materials, *J. Comput. Physics* **169** (2001), 302–323.

[18] S. Hysing, S. Turek, D. Kuzmin, N. Parolini, E. Burman, S. Ganesan, L. Tobiska — Quantitative benchmark computations of two-dimensional bubble dynamics, *Int. J. Numer. Meth. Fluids*

60 (2009), 1259–1288.

[19] B. Lafaurie, C. Nardone, R. Scardovelli, S. Zaleski, G. Zanetti — Modelling merging and fragmentation in multiphase flows with SURFER, *J. Comput. Physics* **113** (1994), 134–147.

[20] M. Meier, G. Yadigaroglu, B.L. Smith — A novel technique for including surface tension in PLIC-VOF methods, *European Journal of Mechanics BFluids* **21** (2002), 61–73.

[21] T. Milcent — Une approche eulérienne du couplage fluide-structure, analyse mathématique et applications en biomécanique, Thèse de doctorat, Université Joseph Fourier, Grenoble (2009).

[22] S. Osher, R. Fedkiw — *Level Set Methods and Dynamic Implicit Surfaces*, Applied Mathematical Sciences, Vol. 153, Springer (2003).

[23] S. Osher, J. Sethian — Fronts propagating with curvature dependent speed: algorithms based on Hamilton–Jacobi formulations, *J. Comput. Phys.* **79** (1988), 12–49.

[24] O. Pironneau — On the transport-diffusion algorithm and its applications to the Navier–Stokes equations, *Numer. Math.* **38** (1981/82), 309–332.

[25] O. Pironneau, M. Tabata — Stability and convergence of a Galerkin-characteristics finite element scheme of lumped mass type, *Int. J. Numer. Meth. Fluids* **64** (2010), 1240–1253.

[26] S. Popinet, S. Zaleski — A front-tracking algorithm for accurate representation of surface tension, *International Journal for Numerical Methods in Fluids* **30** (1999), 775–793.

[27] H. Rui, M. Tabata — A second order characteristic finite element scheme for convection-diffusion problems, *Numer. Math.* **92** (2002), 161–177.

[28] M. Schatzman — *Analyse numérique*, InterEditions (1991).

[29] J.A. Sethian — Level Set Methods and Fast Marching Methods: Evolving Interfaces, in *Computational Geometry, Fluid Mechanics, Computer Vision, and Materials Science*, Cambridge University Press, Cambridge, U.K., (1999).

[30] M. Sussman, P. Smereka, S. Osher — A level set approach for computing solutions to incompressible two-phase flow, *J. Comput. Physics* **114** (1994), 14–159.

[31] R. Temam — *Navier–Stokes Equations. Theory and Numerical Analysis*, Studies in Mathematics and its Applications, Vol. 2, North-Holland (1977).

[32] G. Tryggvason — Numerical simulation of the Rayleigh-Taylor instability, *J. Comput. Physics* **75** (1988), 253–282.

[33] G. Tryggvason, B. Bunner, A. Esmaeeli, D. Juric, N. Al-Rawahl, W. Tauber, J. Han, S. Nas, Y.-J. Jan — A front-tracking method for the computations of multiphase flow, *J. Comput. Physics* **169** (2001), 708–759.